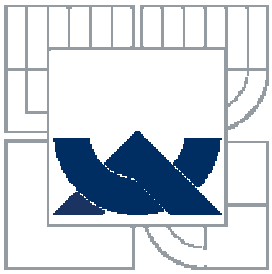

VYSOKÉ UČENÍ TECHNICKÉ V BRNĚ
BRNO UNIVERSITY OF TECHNOLOGY

FAKULTA CHEMICKÁ
ÚSTAV

FACULTY OF CHEMISTRY
INSTITUTE OF

PREPARATION AND CHARACTERIZATION OF SELF ASSEMBLED POLYMER NANOCOMPOSITES

PŘÍPRAVA A CHARAKTERIZACE SAMOUSPOŘÁDÁVACÍCH POLYMERNÍCH NANOKOMPOZITŮ

DIPLOMOVÁ PRÁCE
MASTER'S THESIS

AUTOR PRÁCE
AUTHOR
Bc. PETR LEPCIO

VEDOUCÍ PRÁCE
SUPERVISOR
prof. RNDr. JOSEF JANČÁŘ, CSc.

BRNO 2014

Vysoké učení technické v Brně
Fakulta chemická
Purkyňova 464/118, 61200 Brno 12

Zadání diplomové práce

Číslo diplomové práce:	**FCH-DIP0771/2013**	Akademický rok: **2013/2014**
Ústav:	Ústav chemie materiálů	
Student(ka):	**Bc. Petr Lepcio**	
Studijní program:	Chemie, technologie a vlastnosti materiálů (N2820)	
Studijní obor:	Chemie, technologie a vlastnosti materiálů (2808T016)	
Vedoucí práce	**prof. RNDr. Josef Jančář, CSc.**	
Konzultanti:		

Název diplomové práce:

Příprava a charakterizace samouspořádávacích polymerních nanokompozitů

Zadání diplomové práce:

Nalezení vhodných postupů přípravy polymerních nanokompozitů na bázi PS a PMMA, popis těchto postupů, popis procesů samouspořádávání tuhých nanočástic, charakterizace struktury a vlastností připravených systémů spolu s pokusem o teoretickou interpretaci získaných výsledků.

Termín odevzdání diplomové práce: 9.5.2014

Diplomová práce se odevzdává v děkanem stanoveném počtu exemplářů na sekretariát ústavu a v elektronické formě vedoucímu diplomové práce. Toto zadání je přílohou diplomové práce.

Bc. Petr Lepcio Student(ka)	prof. RNDr. Josef Jančář, CSc. Vedoucí práce	prof. RNDr. Josef Jančář, CSc. Ředitel ústavu

V Brně, dne 31.1.2014

prof. Ing. Jaromír Havlica, DrSc.
Děkan fakulty

ABSTRACT

Polymer nanocomposites based on polyhedral oligomeric silsesquioxanes (POSS) are promising field which could potentially utilize self-assembly approach in designing new materials. In this thesis, a preparation protocol of octaphenyl-POSS/PS, octamethyl-POSS/PMMA and octamethyl-POSS/PS systems was described and thermomechanic properties in solid state and rheological properties in solution were investigated. The obtained results are discussed with focus on nanoparticles dispersion state theories.

ABSTRAKT

Polymerní nanokompozity na bázi polyhedrálních oligomerních silsesquioxanů (POSS) představují slibnou oblast výzkumu, která potenciálně může využít samouspořádávní při navrhování nových materiálů. Tato diplomová práce popisuje postup přípravy oktafenyl-POSS/PS, oktafenyl-POSS/PMMA a oktamethyl-POSS/PS systémů a charakterizaci jejich termomechanických vlastností v pevné fázi a reologických vlastností v roztoku. Získané výsledky jsou diskutovány s přihlédnutím k teoriím zabývajících se stavem disperze nanočástic.

KEYWORDS

Polymer nanocomposites, nanoparticles, self-assembly, state of dispersion, particle spatial organization, thermomechanic properties, rheology, polyhedral oligomeric silsesquioxanes (POSS), polystyrene (PS), poly(methyl methacrylate) (PMMA)

KLÍČOVÁ SLOVA

Polymerní nanokompozity, nanočástice, samouspořádávání, stav disperze, prostorové uspořádání částic, termomechanické vlastnosti, reologie, polyhedrální oligomerní silsesquioxany (POSS), polystyren (PS) polymethylmethakrylát (PMMA)

LEPCIO, P. *Preparation and characterization of self assembled polymer nanocomposites.* Brno: Vysoké učení technické v Brně, Fakulta chemická, 2014. 44 s. Supervisor prof. RNDr. Josef Jančář, CSc..

DECLARATION

I declare that the diploma thesis has been worked out by myself and that all the quotations from the used literary sources are accurate and complete. The content of the diploma thesis is the property of the Faculty of Chemistry of Brno University of Technology and all commercial uses are allowed only if approved by both the supervisor and the dean of the Faculty of Chemistry, BUT.

.....
student's signature

ACKNOWLEDGMENTS

I would like to thank my supervisor prof. RNDr. Josef Jančář, CSc. and the personnel of FCH BUT, namely Ing. Radka Bálková, Ph.D., Ing. Jana Brtníková, Ph.D., Mgr. Zorka Cihlářová, Ing. Ivana Chamradová and Ing. Petr Poláček, Ph.D. for their supervising, advices and help with experimental measurements. Special thanks are addressed to my colleague and friend bc. František Ondreáš for his support.

CONTENT

1. INTRODUCTION

Artificial polymer nanocomposites were first exploited as carbon black filled rubbers for tires and at current state of research and development, they represent an irreplaceable group of materials. Nanoparticles cause nontrivial mechanic response of such composites with a potential for properties enhancement at substantially lower loadings than conventional fillers. It is known that with decreasing size, state of dispersion and molecular interactions grow in importance at the expense of filler bulk mechanical properties which are considered to be irrelevant when reaching sufficiently small scale. Despite the nanocomposites have been studied relatively long up to date, mostly theoretical simulation studies have been carried out to link the nanoparticle spatial organization to macromechanic properties whereas experimental verifications remain scarce and many relations stay hidden and unquestioned.

Polyhedral oligomeric silsesquioxanes (POSS) are interesting group of substances with unusual properties which link together their inorganic silicon-oxygen core with organic moieties, often referred to as 'hybrid'. They possess high variability and since they are defined chemical species they also offer higher regularity than for instance nanosilica. Nowadays, POSS are available as polymer fillers on commercial scale; however, a detailed general structure-property correlation is unknown and the application approach is usually rather semi-empirical.

Self-assembly represents a bottom-up approach for defined nanostructure preparation which could potentially lead to well-organized structures at higher scale levels. Nature has mastered this technique whereas scientists remain amazed and gather inspiration from biological living systems. It allows building up sophisticated structures which connect properties being typically contradictory in conventional materials, e.g. hardness and toughness, all with only few types of building-blocks by getting advantage of the structure assembly. Utilizing this technique could lead to a new generation of self-assembled nanocomposite materials with enhanced properties compared to the current state of art.

2. THEORETICAL PART

2.1. Polymer nanocomposites

Nanocomposites represent a group of composite materials where filler is of nano-size scale (< 100 nm). The possibility to reach a substantial enhancement of properties at very small loadings compared to classical composites has been attracting a wide attention of scientists for a long time. Although some effects are well known, for instance sensitivity of rubber dynamic mechanical response on strain amplitude caused by an addition of carbon black filler, so called Payne effect, a detailed physical understanding of nano-scale structure relation with macroscale properties remains unclear. [1]

2.1.1. Size effect

Size effects are believed to play a crucial role in attempt to understand structure-property relationships in nanocomposites. The surface-volume ratio of particles increases with decreasing particle diameter *D*, thus magnifying the role of interface effects. For example, the average particle distance equals the particle diameter for about 2,6 vol% for randomly packed monodisperse spheres, therefore by assuming a constant interphase thickness of polymer altered by the contact with a particle, we obtain a decreasing fraction of the bulk polymer whereas the proportion of the interphase polymer increases. Eventually, for a common amorphous polymer with radius of gyration $R_g = 5$ nm and particles with $D = 10$ nm there is no residual bulk polymer and all chains are in contact with particles. [1] A simplified view of the situation is shown in Fig. 1.

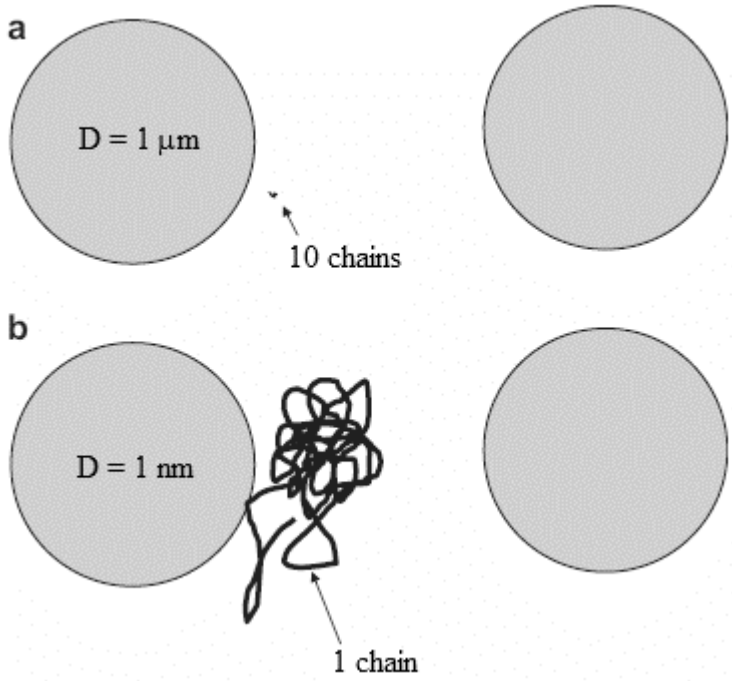

Fig. 1: Schematic difference in the relative size of a polymer chain with R_g = 5 nm compared to (a) microparticles and (b) nanoparticles for average interparticle distance equal to the particle diameter D [1]

A threshold length scale is supposed to exist above which the nano-scale heterogeneities become negligible. It was revealed that the critical size of representative volume element which is usually employed in traditional continuum mechanics modeling is reached when one

of its dimensions drops below approximately 50 nm [1]. Above this limit, conventional fillers were found to reinforce polymer matrices regardless their chemical nature whereas smaller particles can act either as a reinforcement or as a plasticizer [2] because highly attractive nanoparticles slow down chain dynamics and highly repulsive particles accelerate it [1]. The particle size relative to polymer chain was also predicted to affect the particle state of dispersion as is discussed in detail in the chapter 2.1.3.

Dorigato et al. investigated influence of silica nanoparticles on LLDPE elastic modulus and found a dramatic enhancement for increasing specific surface area and filler volume ratio [3]. There are two mechanisms of elastic modulus increase for polymer filled with nanospheres, a volume replacement and molecular stiffening [1]; however, Dorigato et al. concluded that the observed increases cannot be simply explained by stiff interphase formation around particles even for infinitely stiff layers and they attributed this effect to the presence of aggregated nanoparticles. The aggregate mean diameter in one of their samples was determined to approximately 200 nm which is four times higher than the expected critical length. They assumed that the total matrix fraction (ϕ_{m}) is divided between the bulk (ϕ_{m1}) and the constrained matrix (ϕ_{m2}) and that the constrained matrix and filler forms inclusions of volume fraction (ϕ_{i}):

$$\phi_{\mathrm{i}} = \phi_{\mathrm{f}} + \phi_{\mathrm{m2}} \qquad \text{(Eq. 1)}$$

where ϕ_{f} is the filler volume fraction. By introducing a new parameter – the constrained matrix ratio (α):

$$\alpha = \frac{\phi_{\mathrm{m2}}}{\phi_{\mathrm{f}}} \qquad \text{(Eq. 2)}$$

into equations found by Dzenis for a polymer composite with aggregating microparticles they derived the following set of equations for effective bulk (K) and shear (G) moduli which fit the experimental data:

$$K = K_{\mathrm{m}} + \frac{\phi_{\mathrm{i}}\left(K_{\mathrm{f}} - K_{\mathrm{m}}\right)}{1 + \left(1-\phi_{\mathrm{i}}\right)R_{\mathrm{m}}\left(K_{\mathrm{f}} - K_{\mathrm{m}}\right) + R} \qquad \text{(Eq. 3)}$$

$$G = G_m + \frac{\phi_{\mathrm{i}}\left(G_f - G_m\right)}{1 + \left(1-\phi_{\mathrm{i}}\right)Q_m\left(G_f - G_m\right) + Q} \qquad \text{(Eq. 4)}$$

where Q_{m}, R_{m}, Q and R are parameters dependent on the effective bulk and shear moduli of filler and matrix. The indices f and m denote properties connected to filler and matrix respectively. The elastic modulus (E) can be then determined from the expression:

$$E = \frac{9KG}{3K + G} \qquad \text{(Eq. 5)}$$

The detailed description and derivation could be found in the reference 3. However, the authors did not focus closely on the state of dispersion and thus limit the general applicability of their conclusions.

2.1.2. Filler spatial organization

A state of agglomeration could be described by a pair correlation function $G(d)$:

$$G(d) = \frac{V}{N^2}\left(\sum_n \sum_{n \neq m} \delta\left(d - \left|\mathbf{x}_m - \mathbf{x}_n\right|\right)\right) \qquad \text{(Eq. 6)}$$

where N is the number of particles in the examination volume V, $\mathbf{x}_m$ and $\mathbf{x}_n$ denote the position vectors of the particles m and n respectively and δ is the Dirac delta function. It sums

the probability for particles to be located in a certain center-to-center distance d, therefore regular structures result in peaks in $G(d)$ but it is not a correlation function in term of statistics. [4]

A detailed simulation of the nanocomposite behavior demands a considerable computational power and therefore a multiscale modeling which involves methods at different length and time scales is necessary to obtain reasonable computational times. Quantum mechanics deals with scales below 1 nm and 10^{-15} s and it provides bond lengths, bond angles, dihedral angles and force field potentials as its essential parameters. By solving the Schrödinger equation, nuclear and electronic degrees of freedom are determined and described with a many-particle wave function. Atomistic and molecular methods are applicable in range 1–10 nm and 10^{-15}–10^{-9} s and are commonly represented by Monte Carlo simulations or Molecular dynamics. In these methods, the electronic degrees of freedom are replaced by effective coarse-grained interactions between nuclei as described by classical potentials, for instance the Lennard-Jones 6-12 potential, where the choice of potentials should correspond to the interparticle interactions present in the simulated system. Mesoscopic methods (10 nm–10 μm, 10^{-9}–10^{-3} s) are often obtained by coarse-graining the atomistic model where groups of atoms referred to as united atoms or super atoms are treated together. There are two classic particle-based mesoscopic methods tailored for soft matter systems simulations: Brownian dynamics and dissipative particle dynamics; however, both methods are closely related to each other. The Brownian dynamics couples the conservative forces, the particle momentum and Gaussian random noise through the Langevin equation but it does not conserve energy and momentum whereas forces in the dissipative particle dynamics always act pairwise, thus it guarantees the emergence of true hydrodynamic behavior in the limit of a large system size. Techniques which solve continuum mechanics equations either by analysis or by numerical discretization are generally applied at scale above 10 μm and 10^{-3} s, for instance finite-elements, finite-differences or boundary-element method. [5]

The densest packing of monodisperse spherical particles is well-known with face-centered cubic (FCC) and hexagonal close packing (HCP) being the two most common cases. Torquato and Jiao investigated the densest packings of congruent non-spherical particles and pronounced a general tendency of polyhedral particles to increase their face-to-face contact in the densest packing leading to decrease in the particle centroids distance. For both convex and concave shapes, they concluded that the densest packing is given by a corresponding Bravais-lattice for centrally symmetric particles whereas particles which lack central symmetry can exploit rotational degrees of freedom to yield a periodic packing. The most common case is then Bravais-lattice packing of units composed of several particles with inversion-symmetric points. For smoothly shaped particles, they found local principal curvature to play a crucial role with interparticle contact generally favored in area with lower curvature. [6] In connection to nanocomposites, Starr and Douglas performed a molecular dynamics simulation of nanoparticles in bead-spring polymer melt which showed that particles cannot be considered as perfect spheres at nanoscale and their patchiness has to be taken into account. [7]

Colloidal chemistry provides the well-established DVLO theory to describe the agglomeration-dispersion phenomena. Colloidal particles agglomerate due to the van-der-Waals attraction if the Coulomb repulsion, which depends on the ionic strength of the suspension and on the surface charge, as quantified by zeta potential ζ, is not sufficiently

strong to keep them dispersed. For sufficiently strong Coulomb repulsion a primary energy minimum with an energy barrier exists which leads to kinetically controlled agglomeration. For an intermediate ionic strength and a high or intermediate zeta potential, the shallower secondary minimum becomes deeper than 2 k_BT and entraps particles in less stable secondary agglomerates, which stability is more sensitive to particle size than of the primary agglomerates. [4] Although the DVLO theory was originally derived for colloidal electrolytes, it has been extended to other types of interactions to describe different colloidal systems, e.g. hydration forces in case of protein coated polystyrene particles [8].

In polymer nanocomposites, polymer scaffolds can serve three purposes: assembling nanoparticles into clusters, inducing ordering and anisotropic orientation or acting as a functional element. [9] Hooper and Schweizer performed a computational PRISM study on hard spherical particles dissolved in an adsorbing homopolymer melt and predicted four categories of polymer-mediated nanoparticle organization: contact aggregation, steric stabilization, bridging formed by adsorption of more particles on a single chain and "telebridging" where distinct adsorbed layers coexist with longer-range bridging. [10] All types of organization are schematically visualized in Fig. 2.

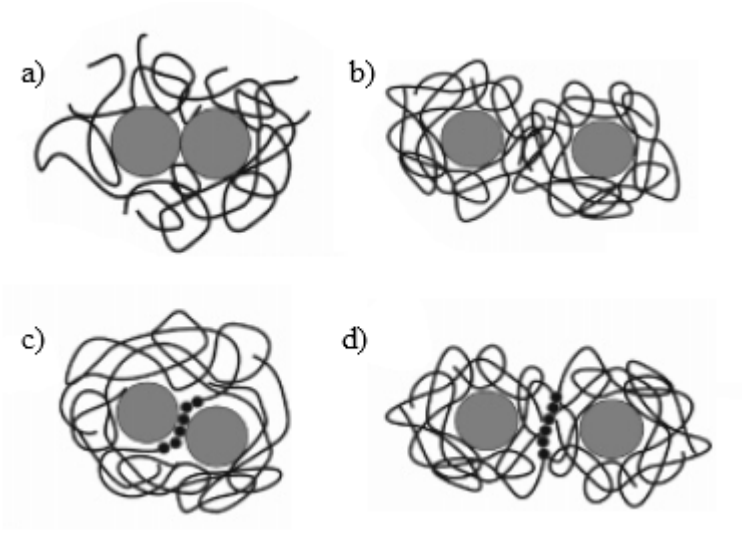

Fig. 2: Schematic visualization of predicted nanoparticle organization modes; a) direct contact agglomeration b) dispersion c) bridging d) telebridging [10]

Hooper and Schweizer found the interfacial polymer-particle strength at contact and spatial-range of particles attraction to play a key role in determining the state of dispersion. A miscibility window for moderate polymer-particle interaction with two types of phase separation was pronounced. The contact aggregation is favored for low affinity between particles and polymer whereas bridging prevails in case of strong attraction. [10] These results were experimentally confirmed by Anderson and Zukoski. [11]. Moreover they reported a gelation for moderate particle interaction strength at higher filler loadings and concluded that the polymer adsorption in the bridged state is reversible and thus the polymer chains can change their configuration on the surface upon cooling.

2.1.3. Effects on spatial organization

Although Hooper and Schweizer predicted a closing and an eventual disappearance of the miscibility window with increasing chain length due to the loss in the polymer translational entropy [10], Anderson and Zukoski observed no evidence for such phenomenon [11]. On the

contrary Patra and Singh reported conservation of the dispersion state independent on particle-chain relative size, a suppression of the direct contact agglomeration for particles bigger than the polymer radius of gyration R_g and decreasing tendency in clustering with increasing chain length for particles smaller than R_g characterized by a sequential shift from string-like to branched and spherical clusters and a cluster dissolution based on their molecular dynamics simulation [12]. The later effect is obviously caused by polymer-induced repulsion forces which first lead to a loss in the particle-particle site preference and eventually completely inhibit the clustering.

According to the simulation, the phase behavior exhibits an entropy-driven lower critical solution temperature type of phase separation and an enthalpy-driven upper critical solution temperature type of phase separation with a miscibility window in-between [10]. Experimental results with three different states of organization were indeed reported by Stenhar et al. [9]. The dispersed state exhibits the highest entropy, followed by the direct contact agglomeration state and the bridged state where both the particle configuration and the polymer confinement between particles contribute to the loss in entropy. The overall potential energy of nanocomposite is dominated by polymer-particle interaction energy and decreases with increasing interaction strength [12]. Douglas and Starr modeled a clustering of nanoparticles in polymer melt with strong short-ranged attractive and weak long-ranged repulsive forces [13] and concluded that such system exhibits a self-assembly transition temperature at which most of the clusters from the low temperature highly-clustered state extinguish and a high temperature highly dispersed state is formed; however, the clusters are partially preserved at higher filler loadings. A diagram of amount of particles in clustered state dependence on temperature for various system densities could be found in the Ref. 13.

To comment on solvation effects, an appropriate physicochemical measure of solvent capabilities is indispensable. Compatibility between polymers and solvents is often described by Hansen's total solubility parameter δ. The solubility parameter concept was first proposed by Hildebrand as the square root of the cohesive energy density:

$$\delta = \sqrt{\frac{\Delta E_{vap.}}{V_m}} \qquad \text{(Eq. 7)}$$

where $\Delta E_{vap.}$ is molar energy of vaporization and V_m denotes molar volume of the liquid. Substances with a $\Delta\delta < 7\ \text{MPa}^{0,5}$ are likely to be miscible, whereas immiscibility is probable with $\Delta\delta > 10\ \text{MPa}^{0,5}$. Hansen separated this one-dimensional parameter into three types of partial solubility which originate from dispersion δ_d, polar δ_p and hydrogen bond δ_h contribution [14]:

$$\delta^2 = \delta_d^2 + \delta_p^2 + \delta_h^2 \qquad \text{(Eq. 8)}$$

In solution, the nanoparticle affinity to polymer must exceed the nanoparticle affinity to solvent for an assembly to occur [9]. Dissolution of nanocomposite induces a dilution of polymer segments and a reduction in repulsive interactions between particles; however, Kim and Zukoski reported that miscibility is not directly tied to solvent quality. At laboratory temperature, particles of a PEG-silica nanocomposite experienced higher repulsive forces in water (good solvent conditions) than in ethanol (near theta-solvent conditions) but at elevated temperature, water (near theta-solvent conditions) segregated to the surface and polymer to the bulk due to the reduced particle repulsion whereas no change appeared in the ethanol (good solvent conditions) solution. [15]

Kalra et al. investigated an influence of shear on nanoparticle dispersion in polymer melts by a coarse-grained molecular dynamics study. They concluded that shear significantly affects the aggregation kinetics, whereas the equilibrium state of dispersion remains unchanged. They claimed that shear induces rupture-like deformation and causes a non-monotonic dependence of diffusivity on shear rate with a critical point at which the decreasing diffusivity turns into increasing with increasing shear rate. The minimum in diffusivity is suppressed for short chains but deepens and shifts to higher shear rates with increasing degree of polymerization. The diffusion constant of small colloid particles with radius smaller than the polymer radius of gyration exceeded the prediction of the Stokes–Einstein equation (see Eq. 12) and exhibited no dependence on polymer molecular weight. [16]

Since nanoparticles are often dispersed in a matrix in thermodynamically non-equilibrium state, a kinetic insight on aggregation phenomena would be more relevant to practical applications; however, only little is known and further research in this field is necessary. Smaller particles experience faster diffusion and therefore also faster aggregation, on the other hand the aggregation rate becomes very slow below the glass transition temperature [17]. The potential of mean force (PMF) exhibits a higher oscillation tendency and more energy wells separated by energy barriers with increasing polymer-particle interaction strength thus leading to an assumption that a formation of kinetic structures dominates the behavior of such systems [12, 17]. This is in agreement with a statement of Stenhar et al. which claims that ionic interactions frequently lead to extended networks arising from kinetic entrapment [9].

2.1.4. Self-assembled systems

Certain similarities could be found across the various self-assembled systems. Since self-assembly is massively utilized in biological living systems, they represent probably the best described non-trivial self-assembly to date. They show four distinct characteristics: *coding* which means that the self-assembly is encoded in each building block, e.g. by monomer sequence, electrostatic charge pattern, hydrogen bonds or hydrophobicity, template which leads to order and asymmetry by introducing constraints and geometrical restrictions to self-assembly, kinetics with both static (equilibrium) and dynamic structures maintained by energy dissipation and hierarchy by associating building blocks (molecules) into larger and more complex objects. [18] Generally, growth of more primitive self-assembled structures up to a certain critical size enables new weaker interactions to come in play, thus causing formation of the next hierarchical level. [19]

Ackora et al. studied a self-assembly of polymer grafted silica nanoparticles – a system which might be simply considered analogical to polyhedral oligomeric silsesquioxanes discussed in detail in the chapter 2.2. They reported a competition between entalpic gain due to particle cores approach and entropy of distorted grafted polymers represented by a short-ranged attraction forces and long-ranged repulsion forces. They observed an assembly of highly anisotropic sheet-like objects for increasing chain length of polymer grafts and/or grafting density on particle surface whereas large aggregates (1–100 μm) formed for non-functionalized or minimally grafted nanoparticles. [20] A similar shift from constrained shape to large aggregates with increasing polymer chain length was proposed by Patra and Singh for nanoparticles blended in polymer matrix as mentioned above. [12]

Polymer grafted nanoparticles were also investigated by Kumar et al. who found an enhanced miscibility of such nanoparticles with matrix of the same chemical composition as the grafts for increasing graft chain length. Further, they proposed that some observed sheet-

like structures are probably kinetically controlled and that anisotropic particles exhibit percolation threshold at lower filler volume ratio than isotropic particles. [21]

2.2. Polyhedral oligomeric silsesquioxanes (POSS)

Silsesquioxanes are a diverse family of chemical substances with empirical formulas $RSiO_{1,5}$, where R refers to an organic chemical moiety or hydrogen. Its history dates back to 1930s when a development research was started in Corning Glass Works and General Electric Company on the basis of academic work by F. S. Kipping. They are known to exhibit different structures including random structure, ladder structure, cage structures and partial cage structure, as illustrated in *Fig. 3*. [22]

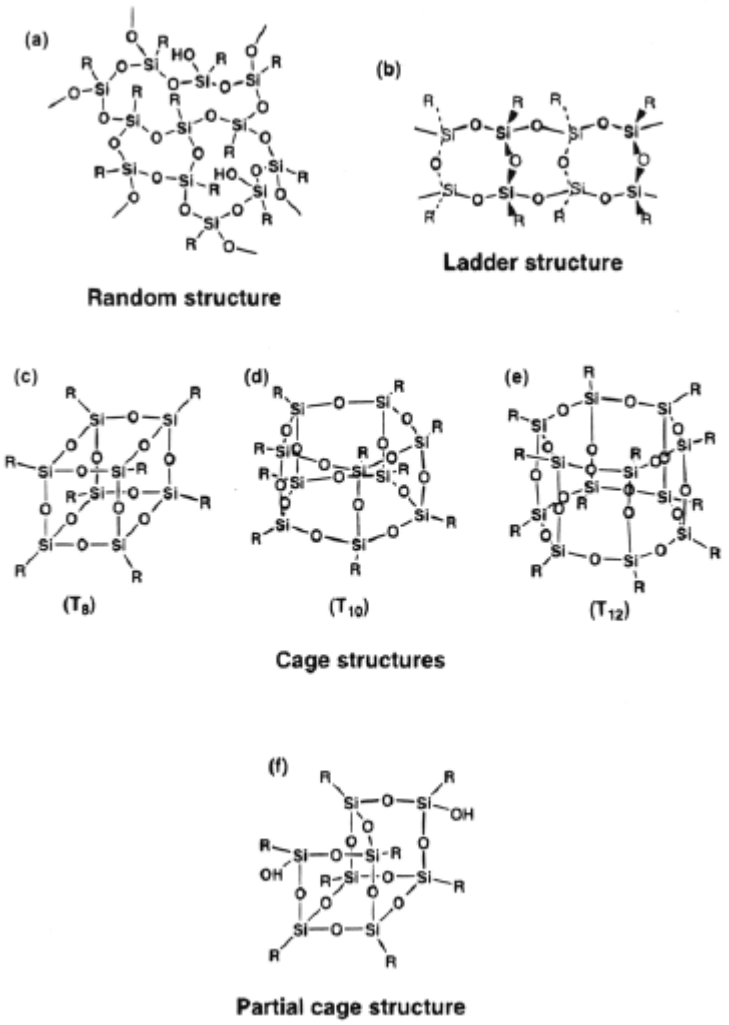

Fig. 3: Structures of silsesquioxanes [22]

Polyhedral oligomeric silsesquioxanes (POSS) consist of an inorganic silica core cage $(SiO_{1,5})_n$ (cages with $n = 8, 10, 12$ were reported) and external organic substituents, which could be represented by any chemical group known in organic chemistry. Different substituents could be present in one molecule, which results in huge number of available POSS variants. This variability together with the POSS well-defined structure compared to nanosilica attracts wide attention of scientists. Nowadays, more than 80 different POSS types including alkyls, olefins, alcohols, esters, anhydrides, acids, amines, imides, epoxies, thiols, sulfonates, fluoroalkyls, silanols, and siloxides are offered for sale by Hybrid Plastics which

owns or controls the basic patents covering synthesis and application of POSS compounds; therefore, it is the only supplier of POSS for commercial use and in cooperation with School of Polymers and High Performance Materials at the University of Southern Mississippi the world leading organization in the field of POSS research. [23, 24]

2.2.1. Synthesis

In general, the classical synthetic approach involves a hydrolysis of trifunctional organo- or hydrosilanes [23, 25–27]. Silsesquioxane $(HSiO_{1,5})_n$ represents the simplest member of the class and it could be employed as a precursor for variety of POSS types preparation [28–30]. It was first synthesized unintentionally by Müller and coworkers in 1959 from trichlorosilane by hydrolysis with sulfuric acid. Frye and Collins developed a new process by hydrolysis of trimethoxysilane [25] and Agaskar and coworkers introduced a new method by hydrolysis of trichlorosilane in scarce-water conditions [26].

Three approaches were reported to synthesize mono- and multifunctional POSS. Cohydrolysis of monomers with different organic moieties (R and R') leads to a mixture of products with all possible R/R' ratios, therefore further separation is necessary in order to receive pure substances [23, 28]. Various methods based on substitution reactions with retention of the siloxane cage were described [23, 28–30], e.g. hydrosilation of the basic hydrido-T_8 unit [29]. The last approach is commonly referred as a corner capping reaction which was first reported by Brown and Vogt [31] and further improved by Feher and Lichtenhan [32, 33] and it is represented by a reaction of monomer with incompletely condensed (T_7) molecules; however, long reaction times and diversity limitations are the major disadvantages of this technique [28]. The methods of monofunctional POSS synthesis are schematically summarized in *Fig. 4*, where Y represents a silane functional group.

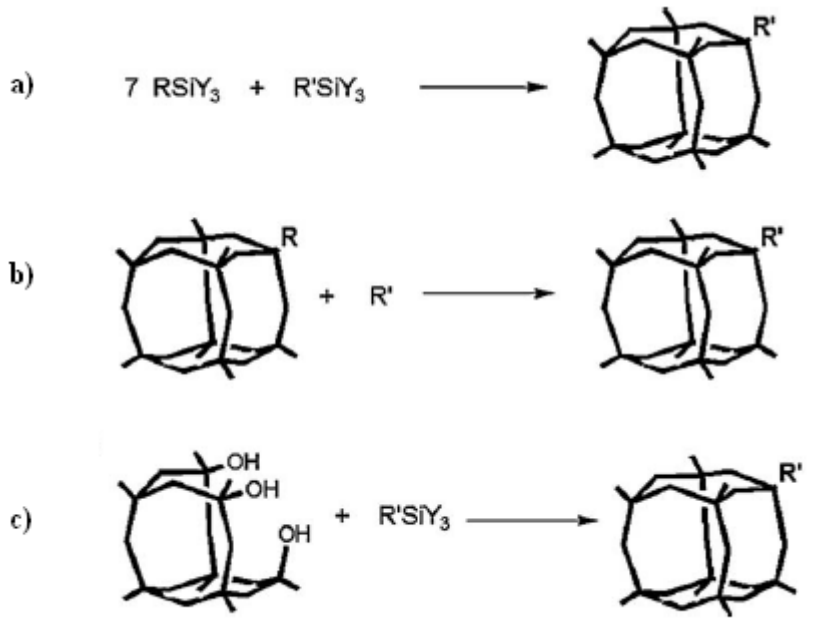

Fig. 4: Methods of monofunctional POSS synthesis, a) Cohydrolysis of different monomers, b) Substitution reaction, c) Corner capping reaction [23]

2.2.2. Properties

POSS unique properties origin in its hybrid organic-inorganic structure and predominantly depend on its R substituents attached to the inorganic core [23, 34–36] including its compatibility and solubility in solvents. POSS are mostly solid white powders and some are colorless liquids. The powder particles possess diameter typically between 1–100 microns; however, in solvents POSS forms entities ranging from 1–3 nanometers to micron-sized domains according to its compatibility with the specific solvent. POSS nanostructures can be considered as the smallest possible particles of silica; however, despite its common reference as molecular silica, POSS have lower densities (0.97–1.82 $g \cdot cm^{-3}$ compared to 2.60 $g \cdot cm^{-3}$ of quartz) and are less abrasive with Mohs hardness of approximately 1. [23, 24]

Unlike many organic compounds, POSS are nonvolatile, odorless and environmentally friendly substances. Their acute oral toxicity belongs to the lowest category both in the European Union (LD50 ≤ 2 000 mg/kg pursuant to the Regulation (EC) 1272/2008) and in the USA (LD50 ≤ 5 000 mg/kg pursuant to the Toxic Substances Control Act) regarding to the performed toxicity tests; however, results are not available for all types of POSS and further testing is being carried out. [23, 24]

2.2.3. POSS in polymeric materials

Nowadays, POSS additives dedicated to polymeric materials are available on commercial scale. Hybrid Plastics' manufacturing facility manages capacity in the hundreds of metric tons per year range. POSS substituents on their surface could be tailored to provide miscibility with most polymers without any further surface treatment; however, a fundamental description of non-equilibrium POSS nanoparticles self-assembly and its influence on a polymeric matrix on the molecular scale remains a riddle. In addition, POSS could be physically blended in a polymeric matrix as common fillers by solution or melt blending or covalently bonded to a polymer chain through reactive functional groups what consequents to several POSS/polymer architectures as shown in *Fig. 5*. [23, 24]

Tuning the POSS substituents is a well-established method in tailoring the POSS/polymer nanocomposite properties with close impact to miscibility and dispersion state of the nanoparticles [34–37]. Blends with fully dispersed nanoparticles at a molecular scale [36] as well as POSS-domains formation of various sizes were reported [35–39] and the diversity is further pronounced by existence of both crystalline [35, 36] and amorphous-nature of the domains [35, 39].

Kuo and Chang investigated an influence of hydrogen bonding on miscibility between POSS core and phenolic group on model compounds octaisobutyl-POSS and 2,4-dimethylphenol. The free energy of mixing two polymers ΔG_m could be expressed by Flory–Huggins equation with Painter and Coleman supplement [40] which accounts the free energy of hydrogen bond formation contribution ΔG_H:

$$\frac{\Delta G_m}{RT} = \frac{\phi_A}{M_A} \ln \varphi_A + \frac{\phi_B}{M_B} \ln \varphi_B + \phi_A \phi_B \chi_{AB} - \frac{\Delta G_H}{RT} \qquad \textit{(Eq. 9)}$$

where ϕ_A and ϕ_B are volume fractions of the polymers, M_A and M_B are the corresponding degrees of polymerization and χ_{AB} denotes the interaction parameter. By employing the Coggeshall and Saier equation:

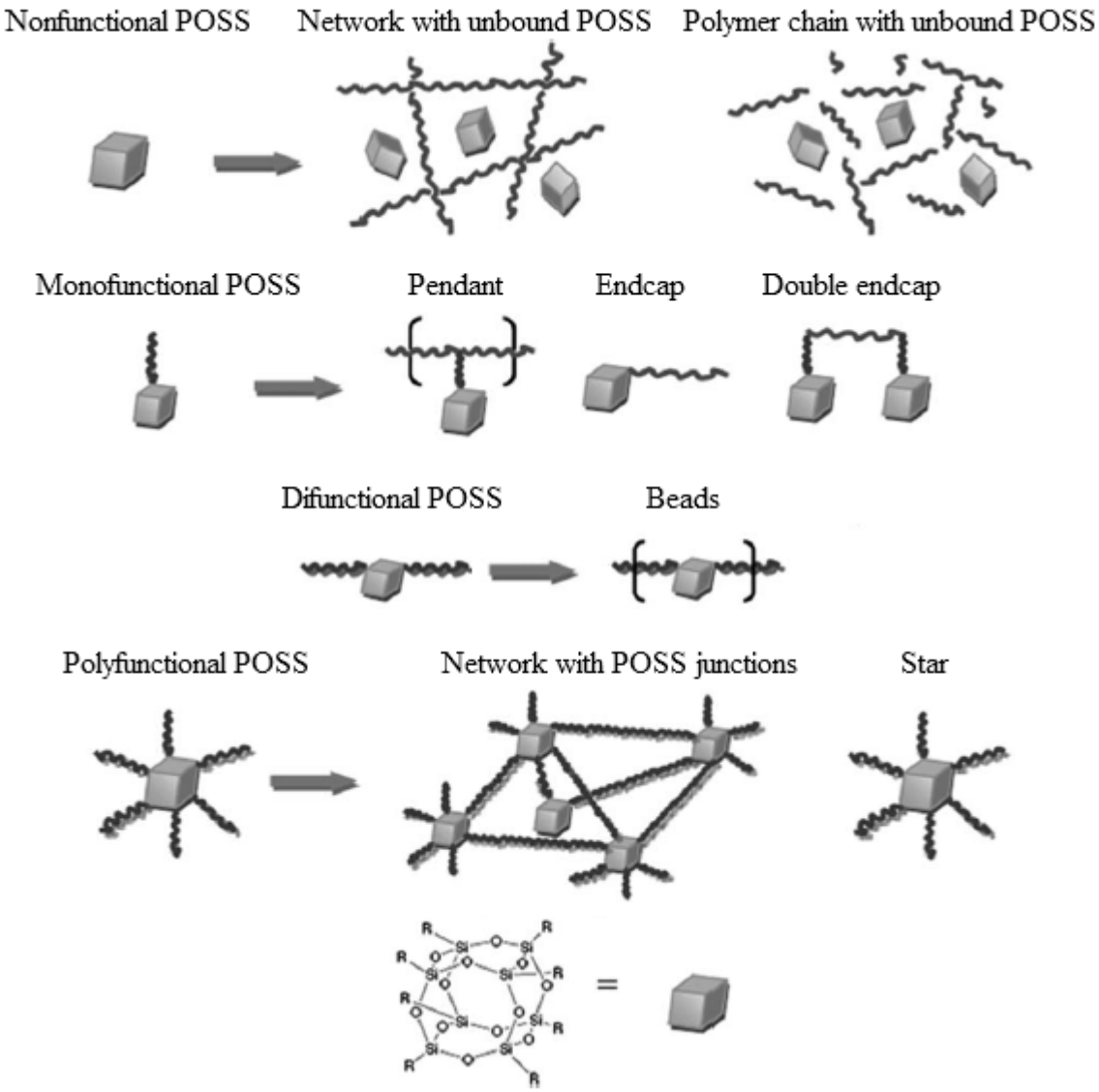

Fig. 5: POSS/polymer architectures [23]

$$K_a = \frac{1 - f_m^{OH}}{f_m^{OH}\left(C_A - \left(1 - f_m^{OH}\right)C_B\right)} \qquad \textit{(Eq. 10)}$$

where K_a is the equilibrium constant for the hydrogen bond association, C_A and C_B are the concentrations (in $mol \cdot l^{-1}$) and f_m^{OH} is the fraction of free bond-donating group; which is built in the Painter-Coleman association model [40], Kuo and Chang estimated that Novalic type phenolic resin self-association equilibrium constant (52.3) exceeds the equilibrium constant of hydrogen bond formation between phenolic OH group and POSS Si–O–Si group (38.7). Despite its positive contribution, the hydrogen bonding between POSS core and phenolic resin provides only partially miscible or immiscible mixtures and hydrogen bond accepting substituents are necessary to enhance the POSS-phenolic miscibility. [23]

Hybrid Plastics advertises two main cases of POSS advantage, the first represented by an improved performance unachievable or only intricately achievable by any other technique and the second based on a reducing of a filler loading amount due to the POSS higher efficiency which results in bearable prices despite its higher specific expenses [24]. The influence of POSS additives on polymer properties is diverse as the POSS family itself, for instance they can affect thermomechanical properties by plasticizing [36] and antiplasticizing [41], improve

thermal properties by SiO_2 protective layer formation [34], increase gas permeability [42], lubricate or cause a gelation [43] or they lead to shape-memory [38] and self-healing materials [36]. They also modify a polymer crystallinity and crystallization kinetics of semicrystalline polymers with possibility acting as a nucleating agent or as a growth center which induces and enhances the polymer polymorphism [37, 43].

2.3. Analytical methods

2.3.1. Dynamic light scattering

Particle sizes and shapes can be determined by detection of electromagnetic radiation scattered by the particles. In suspension, particles move with Brownian motion and therefore the scattered radiation experiences the Doppler shift. Diffusion coefficients and thus measure of size of particles can be calculated from the shift in wavelength. [44]

In dynamic light scattering technique, coherent light produced by a laser is focused to small volume and scattered by particles in dilute dispersion. The dilution is necessary to preserve random structure which provides random scattering. The intensity detected by a photomultiplier fluctuates due to the motion of the particles during the total time of the measurement which is termed correlation delay time τ_c. The instrument constructs an exponentially decaying correlation function:

$$g(\tau_c) = \exp\left(-\tau_c D_s Q^2\right) \qquad \text{(Eq. 11)}$$

where D_s is the self-diffusion coefficient of the particle and Q denotes the magnitude of the scattering vector. The correlation delay time is then found as a slope of natural logarithm plotted against Q^2. The hydrodynamic radius of the particle a_H is given by the Stokes-Einstein equation:

$$a_H = \frac{k_B T}{6\pi\eta_0 D_s} \qquad \text{(Eq. 12)}$$

where η_0 is the viscosity of the continuous phase, k_B is the Boltzamann constant and T is the thermodynamic temperature. The hydrodynamic radius corresponds to microscopic observations if the particles are hard spheres but gives higher values for non-spherical particles or particles covered with a stabilizer layer of non-negligible thickness. For polydisperse particles, the correlation function becomes the sum of each of the exponential decaying terms. Due to this problem the sum cannot be solved by simple function inversion and therefore the method is calibrated against particles of known size. [44]

2.3.2. Thermogravimetric analysis (TGA)

Thermogravimetric analysis uses thermobalance to measure the mass and change in mass as a function of temperature, time or both. Mass changes are invoked by processes such as sublimation, evaporation, decomposition, chemical reaction, adsorption or desorption and these are influenced by heating rate and by the choice of purge gas. Both inert and oxidative gases are commonly used, typically oxygen, air, nitrogen and helium. [45]

Heating program significantly influences the obtained thermogravimetric curve. Both ramping and isothermal measurements can be conducted and proper combination of these phases enhances resolution of superposed effects. In addition, switching purge gases during the measurement can also provide additional information on sample properties. The final temperature for a plastic analysis lies typically between 600 and 1000 °C. [45]

2.3.3. Fourier transform infrared spectroscopy (FTIR)

Infrared radiation (IR) is a section of electromagnetic radiation with wavenumber $\tilde{\nu}$ ranging from approximately 200 to 4000 cm^{-1}. The relation between the wavenumber, wavelength λ, frequency f, and angular frequency ω is given by the following equation:

$$f = \frac{1}{\lambda} = \frac{\tilde{\nu}}{c} = \frac{\omega}{2\pi c} \qquad \text{(Eq. 13)}$$

where c denotes the light velocity in vacuum. Absorption of IR leads to excitation of specimen oscillation state which invokes peaks in absorbance as a function of the wavenumber. Several oscillation modes are possible: symmetrical and antisymmetrical stretching, scissoring, rocking, wagging and twisting. [46, 47]

In Fourier transformed infrared spectroscopy (FTIR), a source light beam is split into two parts with a continually varying phase difference. One of the beams interacts with sample and the interference signal after recombination with the second beam is recorded as an interferogram. An infrared spectrum is then calculated with a Fourier transform. The main advantages of this technique are the simultaneous record of whole spectra which provides maximum efficiency and more conventional optical geometry than dispersive infrared instruments. Several consequences arise from these factors, for example higher signal-to-noise ratio, higher resolution or faster measurement. [46, 47]

2.3.4. Differential scanning calorimetry (DSC)

Calorimetry is a technique for determining the quantity of heat that is either absorbed or released during a physical or a chemical change. The heat flow is measured as a function of temperature and/or time. Exothermic processes (crystallization, curing, decomposition) result in increased heat flow whereas endothermic (melting, evaporation, glass transition) decrease it (see Fig. 6). [45]

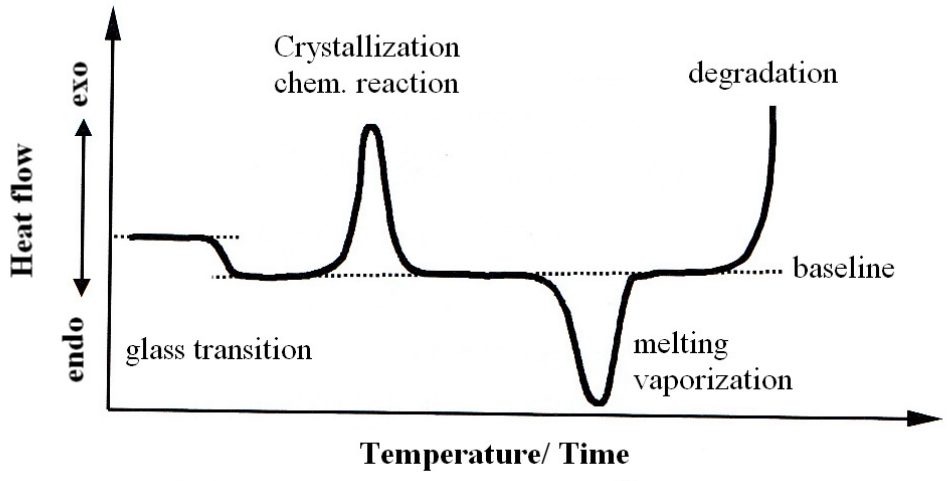

Fig. 6: Typical DSC responses for processes common in thermoplastic polymers [45]

Two measuring methods are known, heat-flux DSC and power-compensation DSC. In the heat-flux DSC, reference and sample are heated and cooled together in one furnace and the difference in their heat fluxes cause different respond to the dynamic temperature program. In the power-compensation DSC, reference and sample are placed in two separated and independently controlled furnaces which are maintained in a "thermally null" state by

compensating power supplied to the specimen furnace. However, both methods yield comparable information and both are commonly referred to as DSC. [45]

2.3.5. Dynamic mechanical analysis (DMA)

Dynamic mechanical analysis (DMA) provides information about the mechanical properties of a specimen placed in minor, usually sinusoidal, oscillation as a function of time and temperature. The applied stress invokes a corresponding strain whose amplitude and phase shift δ is measured. The deformation is related to the stiffness of the material which is described by the complex modulus E^* composed of two perpendicular parts, the storage modulus E' (real part) and the loss modulus E'' (imaginary part). The ratio of loss modulus to storage modulus is referred to as the loss factor tan δ. [45]

Below the glass transition temperature T_g, molecules of amorphous thermoplastics are in glassy state, immobile and unable to resonate with oscillatory loads. At elevated temperatures, rubbery or entropy elastic state is reached and the storage modulus decreases- When the timescale of molecular motion coincides with that of mechanical deformation, oscillation is converted into the maximum internal friction and non-elastic deformation and loss modulus reaches its maximum. The loss factor also experiences a maximum, but since the storage modulus decreases, its increase is initially suppressed and the maximum is shifted towards higher temperature than in case of the loss modulus, as shown in Fig. 7. [45]

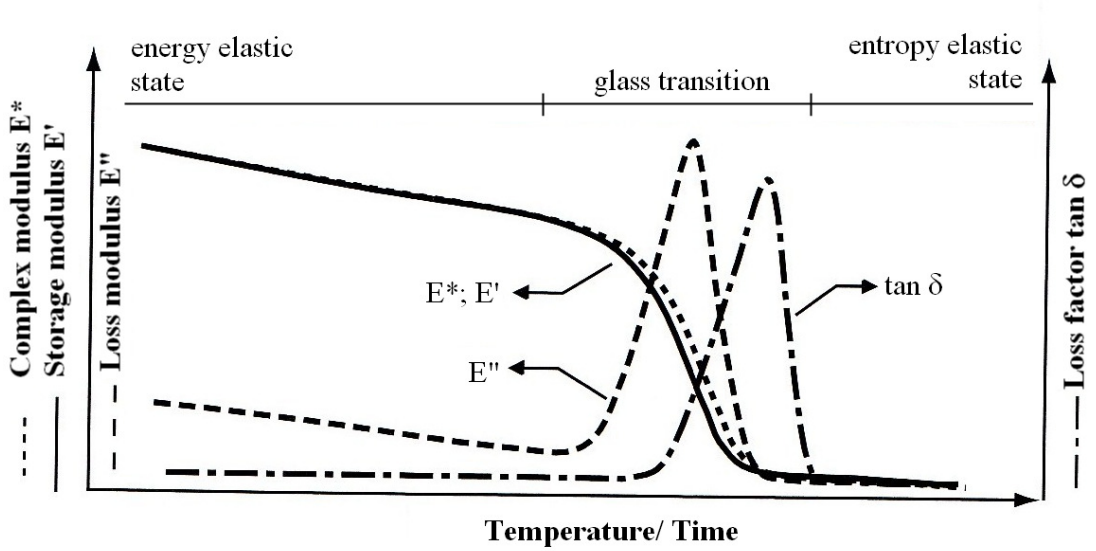

Fig. 7: Typical DMA results for thermoplastic polymers [45]

2.3.6. Scanning electron microscopy (SEM)

Scanning electron microscopy (SEM) is a microscopic method which employs electrons to visualize surfaces with higher magnification than is reachable by light microscopy. The qualitative and quantitative information is extracted by energy-dispersive x-ray spectrometer (EDS) or by wavelength-dispersive x-ray spectrometer (WDS). [48, 49]

An incident electron beam from an electron source which might be for instance a heated tungsten filament or a field emission cathode is focused on to the specimen by electromagnetic lenses and scanned over its surface in a raster pattern. The incident electron energy typically ranges from 100 eV to 30 keV and the beam can be focused to a final probe

diameter as small as about 10 Å. The SEM column and sample chamber are evacuated to avoid unwanted electron scattering. Non-conducting samples are sputtered with a thin conductive layer to reduce electrical charging induced by the electron beam. [48, 49]

Different types of response which result from the incident electrons-specimen interaction provide several scanning modes. High-energy backscattered electrons arise from an elastic collision of the incident electron and a sample atom's nucleus. They provide contrast as a function of elemental composition, because the amount of backscattered electron is proportional to the mean atomic number. Heavier atoms backscatters more electrons and thus appear lighter on the SEM image in this mode. Secondary electrons are emitted by inelastic scattering from the sample atom's electron shell and possess lower energy than the backscattered electrons. The depth from which they can escape the sample is much lower than in case of the backscattered electrons thus the intensity of detected electrons is more sensitive to surface topology and contrast provided by these local variations gives fine images of surface morphology. Collisions can also lead to excitation of electrons from sample atom's electron shell to higher energetic levels. Their relaxation emits x-rays which are detected by the EDS or the WDS. Sometimes the electron relaxation to lower energetic level is accompanied by release of a low-energy electron from the same atom and these are referred as Auger electrons. [48, 49]

3. EXPERIMENTAL PART

3.1. Chemicals

The applied chemicals are summarized in Table 1. Octaphenyl-POSS (OP-POSS) and octamethyl-POSS (OM-POSS) with T_8 core structure were used as obtained from Hybrid Plastics. They are both white inert powdery solids with densities 1,35 g·cm^{-3} and 1,50 g·cm^{-3} respectively [24]. Polystyrene Krasten 154 (PS, Synthos Kralupy) and poly(methyl methacrylate) Plexiglas 8C (PMMA, Evonik) were utilized as polymer matrices. Toluene and acetone were supplied by Lach-ner in pro-analysis purity grade. For initial experiments, tetralin (1,2,3,4-tetrahydronaphthalene, Deza, purity > 96 %) was employed for its advantage of having the same value of solubility parameter (19,4 J^{0,5}·cm$^{-1,5}$) as PMMA. [50].

Table 1: Chemical substances overview [24, 50]

Substance		Appearance	ρ (g·cm^{-3})	δ (J^{0,5}·cm$^{-1,5}$)
OM-POSS	Octamethyl-POSS	white powder	1,50	
OP-POSS	Octaphenyl-POSS	white powder	1,35	
PS	Polystyrene	granulate	1,05	18,6
PMMA	Poly(methyl methacrylate)	granulate	1,20	19,4
	Acetone	colorless liquid	0,79	19,9
	Toluene	colorless liquid	0,87	18,2
	Tetralin	yellowish liquid	0,97	19,4

3.2. POSS suspensions

POSS behavior in solvent was investigated to eliminate the influence of polymer matrix. To estimate compatibility with PMMA and PS, sedimentation tests were performed in tetralin and in mixtures of toluene and acetone with different volume ratios respectively. The following concentrations of POSS with respect to solvent were examined: 0,1 wt.%, 1,0 wt.% and 10 wt.%. The suspensions were stirred mechanically and dispersed ultrasonically with Bandelin Sonoplus homogenizator with 0,6:0,2 on:off pulsation period for 2 minutes. Samples of OP-POSS in the toluene-acetone mixture exhibited milky haze appearance which evidenced a colloid dispersion and therefore the particle size was measured by mean of dynamic light scattering with Zetasizer 3000HS with light beam of wavelength 633 nm. Before the measurement, the samples were dispersed in-situ by ultrasound.

3.3. POSS nanocomposites

OP-POSS/PS nanocomposites with POSS concentration ranging from 0,1 to 10,0 wt.% were prepared by solution blending in toluene and toluene/acetone mixture with various volume ratios. OM-POSS/PS and OP-POSS/PMMA samples with 1,0 wt.% were prepared analogically to compare contribution of specific interactions between polymer matrix and filler. Initial experiments with tetralin and PMMA were performed but they were soon abandoned due to inability to evaporate the solvent entirely while avoiding polymer degradation which is supposed to be consequence of the relatively high tetralin boiling point (206,9 °C [50]) and high PMMA-tetralin affinity.

Firstly, polymer was dissolved at a constant polymer/solvent ratio of 1 g per 7,5 ml of solvent under reflux distillation at 75 °C (Fig. 8A), mixed with POSS, dispersed ultrasonically

with Bandelin Sonoplus homogenizator with 0,6:0,2 on:off pulsation period for 2 minutes while stirred with a magnetic stirrer and dried at 80 °C for 3 hours and then for next 16 hours under vacuum to create POSS masterbatches of approximately 70 wt.% of POSS as was verified by TGA. An evidence of residual solvent presence was found; however, since the masterbatches were intended for further solution blending application, they were not further dried. In the next step, nanocomposites were prepared similarly to the description above with certain variations – masterbatches were utilized instead of pure POSS and the samples were first dried at 80 °C for 1 hour and for 16 hours under vacuum (Fig. 8B), grinded, entirely dried under vacuum at 140 °C for 2 hours (Fig. 8C) and grinded again (Fig. 8D). Blanc samples were prepared analogically. Few pieces of the grinded 10 % of OP-POSS/PS nanocomposite were attached to a holder (Fig. 9) and observed in Tescan (Brno, Czech republic) with MIRA3 SEM by applying accelerating voltage 3,0 kV in so-called 'Enviro mode' – under low vacuum without any coating treatment.

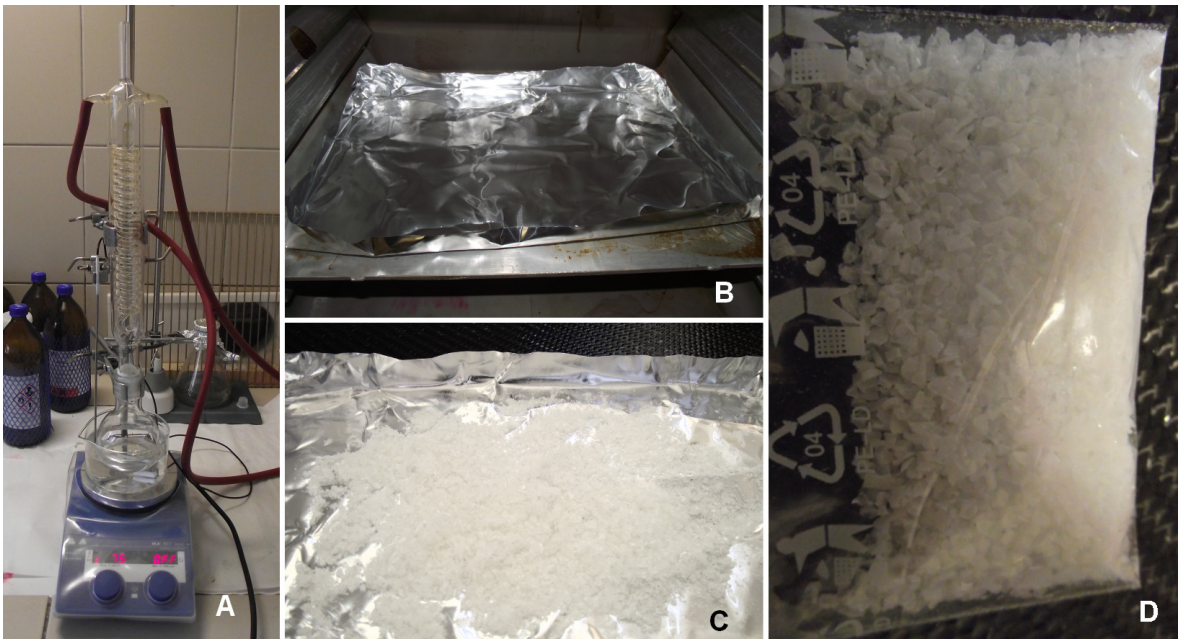

Fig. 8: Nanocomposite preparation; A – polymer dissolution, B – first drying, C – residual solvent evaporation, D – nanocomposite after grinding

Thermogravimetric analysis was performed with TGA TA Instruments Q 500. Typical sample mass ranged between 10–15 mg but higher loadings up to 50 mg were used for composites with low POSS concentrations. Blanc samples and samples with OM-POSS were heated in nitrogen to 500 °C with rate 10 °C·min^{-1}, samples containing OP-POSS were first heated in nitrogen to 800 °C with rate 10 °C·min^{-1}, the purge gas was switched to compressed air and the program ended with 10 minutes isothermal step.

IR spectra were measured with FTIR Bruker Tensor 27 in the middle IR range (4 000–400 cm^{-1}) in the transmission mode on KBr pellets and compared with the FTIR tabulated values in Ref. 51–54. DSC was measured with Netzsch F1 204 heat-flow calorimeter from –30 °C to 130 °C with heating rate 10 °C·min^{-1}, first and second heating were performed on each sample, the cooling phase was not evaluated. The typical sample mass ranged between 10–13 mg.

Fig. 9: 10 % OP-POSS/PS nanocomposite attached to a holder for SEM

Nanocomposite sheets of approximate thickness 0,35 mm were produced by press-molding with Fontune Presses LPB 300 by preheating to 200 °C for 5 minutes and then pressing to 300 kN for 2 minutes. The nanocomposite sheets were observed with confocal laser scanning microscope Olympus LEXT OLS3000.

Specimens for DMA were cut from the nanocomposite sheets in form of bars with dimensions (30×2×0,35) mm and DMA was performed with TA Instruments RSA G2 in a tensile configuration. First, strain amplitude 0,02 % was chosen from linear region of strain sweep measurements which were conducted for strain ranging from $1 \cdot 10^{-3}$ % to 0,5 %. Then, temperature ramp measurement were carried out from 40 °C to 120 °C with heating rate 3 °C·min^{-1}. For all measurements, frequency 1 Hz and loading gap 10 mm were applied.

Rheological behavior was studied with TA Instruments AR G2 rheometer with cone-plane geometry (cone diameter 40 mm, cone angle 2°) on samples prepared by nanocomposites dissolution in toluene with sample-solvent ratio 1:5 and 1:2,5 g/ml. Each sample was dispersed for 5 minutes in ultrasonic bath Kraintek K5 one hour prior the measurement. The tests were then performed in oscillatory regime by varying the applied strain from 0,01 to 10 000 % at frequency 1 Hz and temperature 25 °C which was maintained by Peltier module.

4. RESULTS AND DISCUSSION

4.1. POSS suspensions

Samples with concentrations 0,1 wt.%, 1,0 wt.% and 10,0 wt.% of OM-POSS and OP-POSS in tetralin were investigated to estimate the POSS compatibility with PMMA according to the same Hansen solubility parameters of PMMA and tetralin (19,4 $J^{0,5} \cdot cm^{-1,5}$). 10,0 wt.% OP-POSS is shown in Fig. 10 as the most outgoing example but similar behavior with rapid sedimentation after initial dispersion was observed for all concentrations of OP-POSS. On the contrary, OM-POSS did not form a milky hazed suspension and instead remained in aggregates observable by naked eye (Fig. 11), thus implying that tetralin affinity to OM-POSS is lower than to OP-POSS.

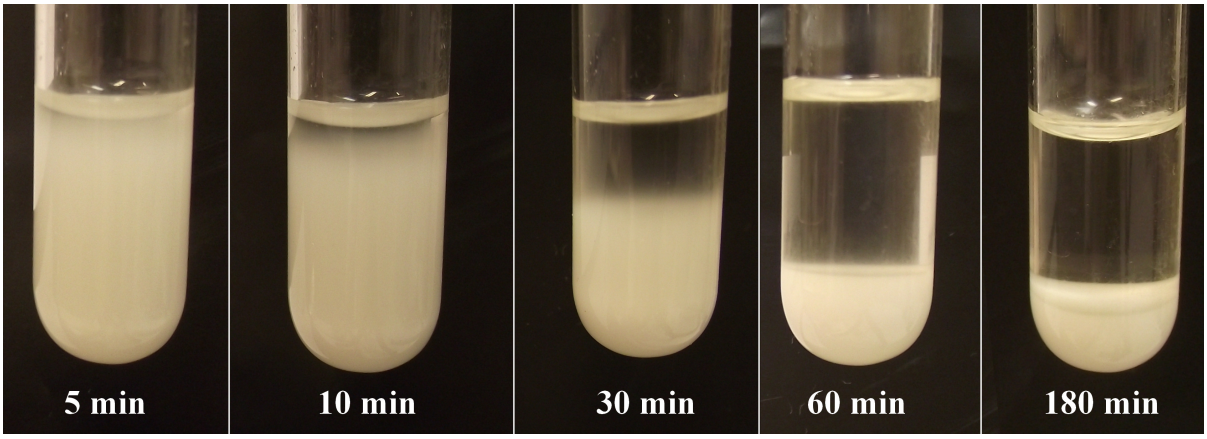

Fig. 10: Sedimentation of 10 wt.% OP-POSS in tetralin

Dynamic light scattering of OP-POSS colloidal suspension proved presence of nanometer-scale particles with the mean size roundly about 20 nm and the smallest determined particle size of 2,4 nm which is approximately two times the POSS-unit diameter. The particle mean size experienced low dependence on the solvent mixture composition with rather high standard deviation caused by the particle polydispersity. Since the Hansen's solubility parameter does not show a monotonic dependence on the mixture composition (see Fig. 12), the particle mean size was plotted in Fig. 13 as a function of Hansen's solubility parameter of the suspending liquid.

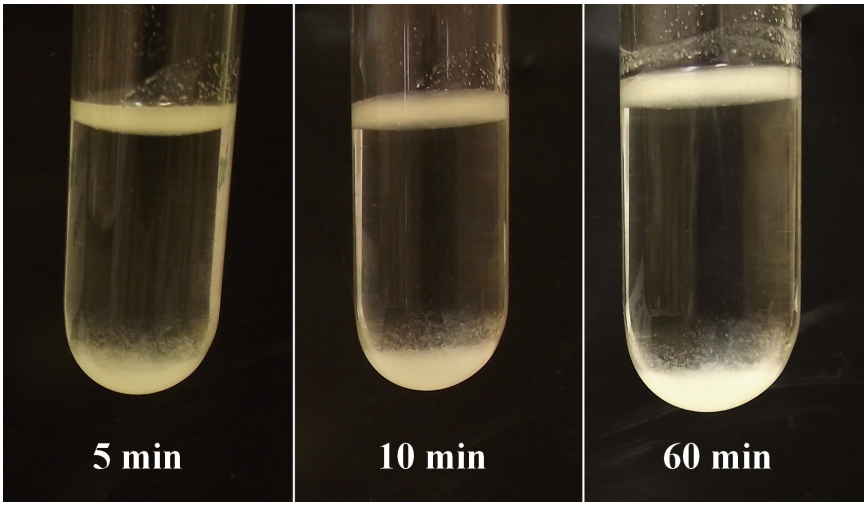

Fig. 11: Sedimentation of 10 wt.% OM-POSS in tetralin

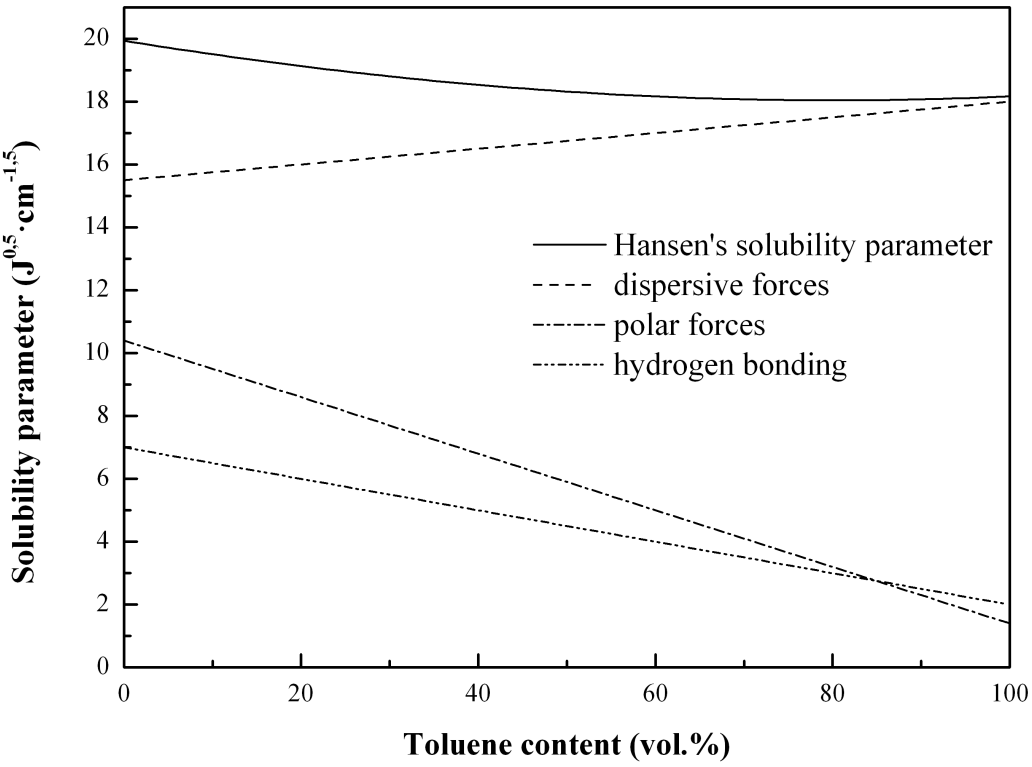

Fig. 12: Hansen's solubility parameter of toluene/acetone mixture

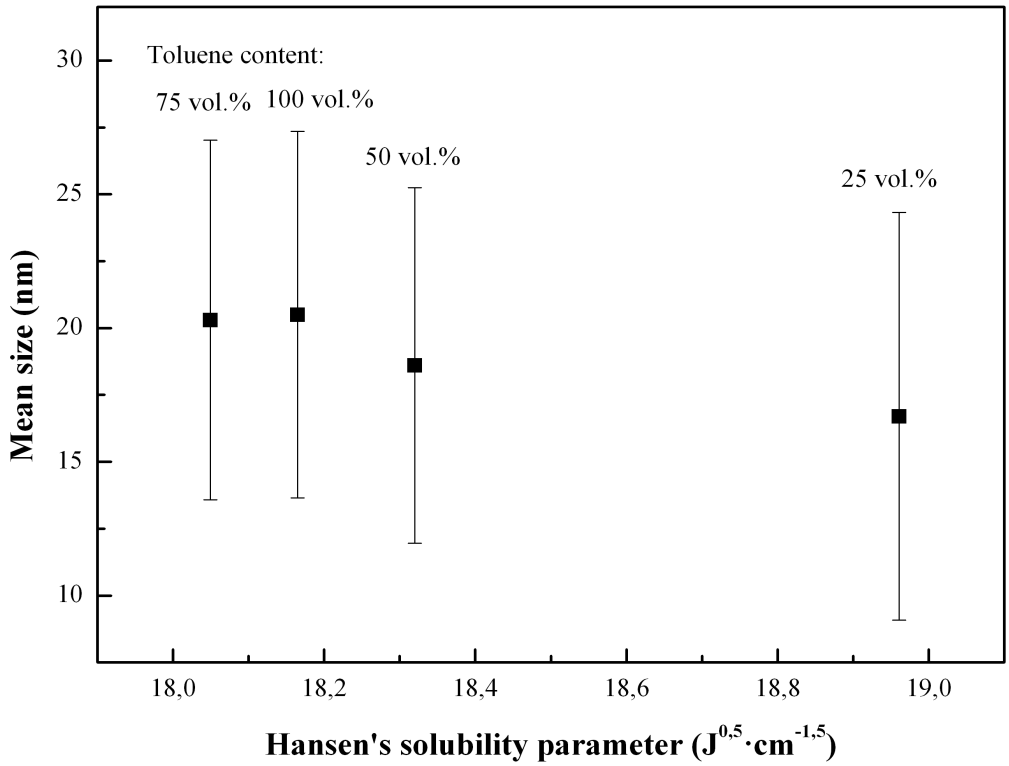

Fig. 13: OP-POSS particle mean size dependence on Hansen's solubility parameter

4.2. POSS nanocomposites

4.2.1. Thermogravimetric analysis

Thermogravimetric records of pure OP-POSS and OM-POSS are shown in Fig. 14 and Fig. 15 respectively. According to these charts, one might think that substituting methyls to phenyls on the POSS-core leads to substantial difference in the thermal decomposition temperatures about 500 °C; however, another test was performed by maintaining OP-POSS at 450 °C to prove that OP-POSS higher thermal resistance is caused by slower kinetics of its decomposition. Two initial steps followed by slow linear weight decrease were found as shown in Fig. 16.

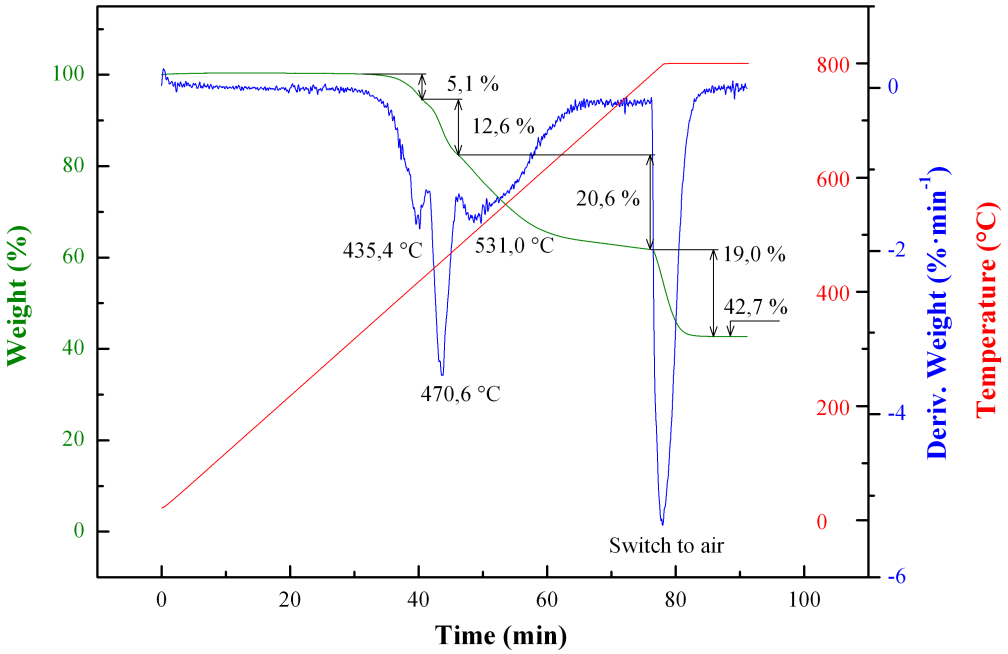

Fig. 14: Thermogravimetric analysis of OP-POSS

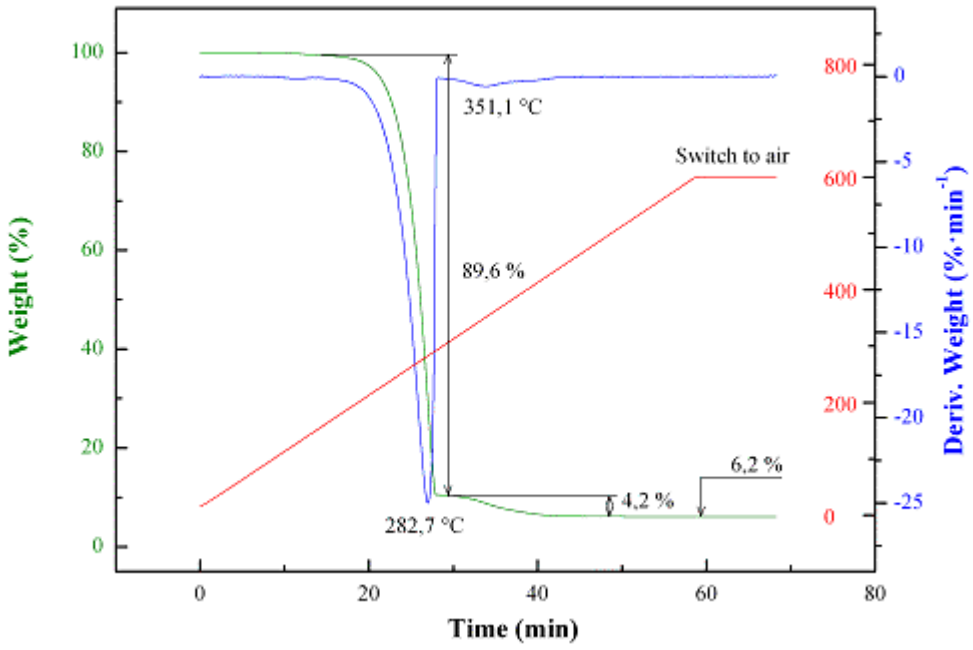

Fig. 15: Thermogravimetric analysis of OM-POSS

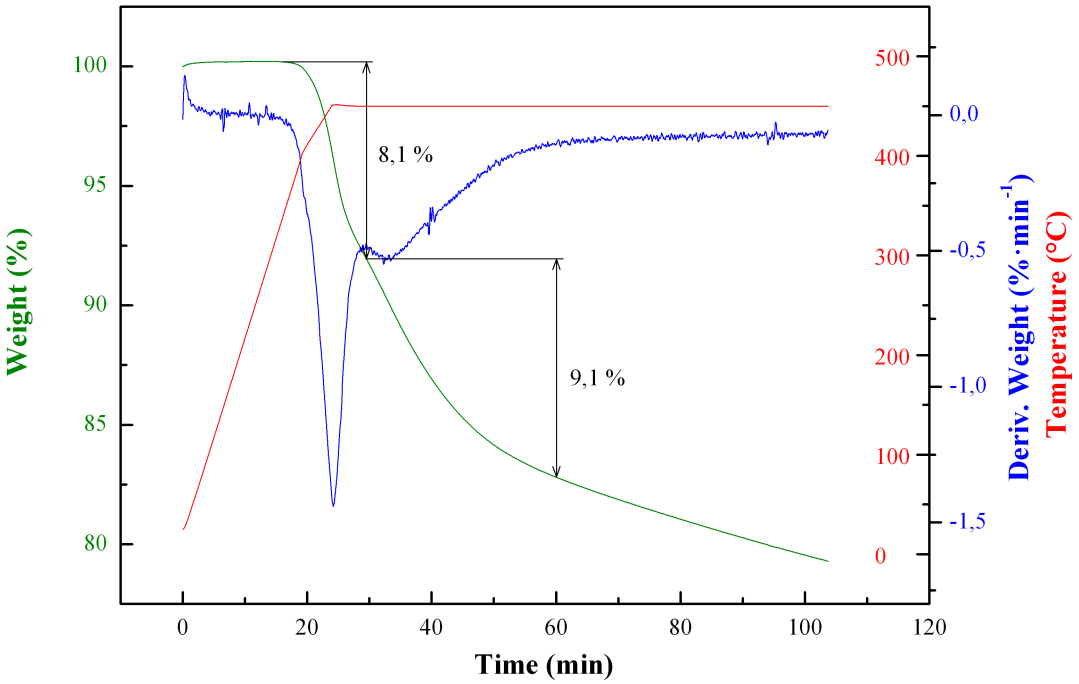

Fig. 16: TGA record of OP-POSS maintained at 450 °C

TGA proved well in determining POSS content at higher POSS loadings; however, its sensitivity is insufficient for POSS loadings 1,0 wt.% and lower with no trace of POSS presence. Fig. 17 is presented as an example of OP-POSS/PS/toluene system with all components clearly distinguishable from each other. The obtained values 8,0 % of toluene, 21,2 % of PS and 70,8 % of OP-POSS were applied to calculate the batch sizes for the nanocomposite samples. TGA also proved efficiency of the applied drying process by showing no traces of weight decrease below 150 °C.

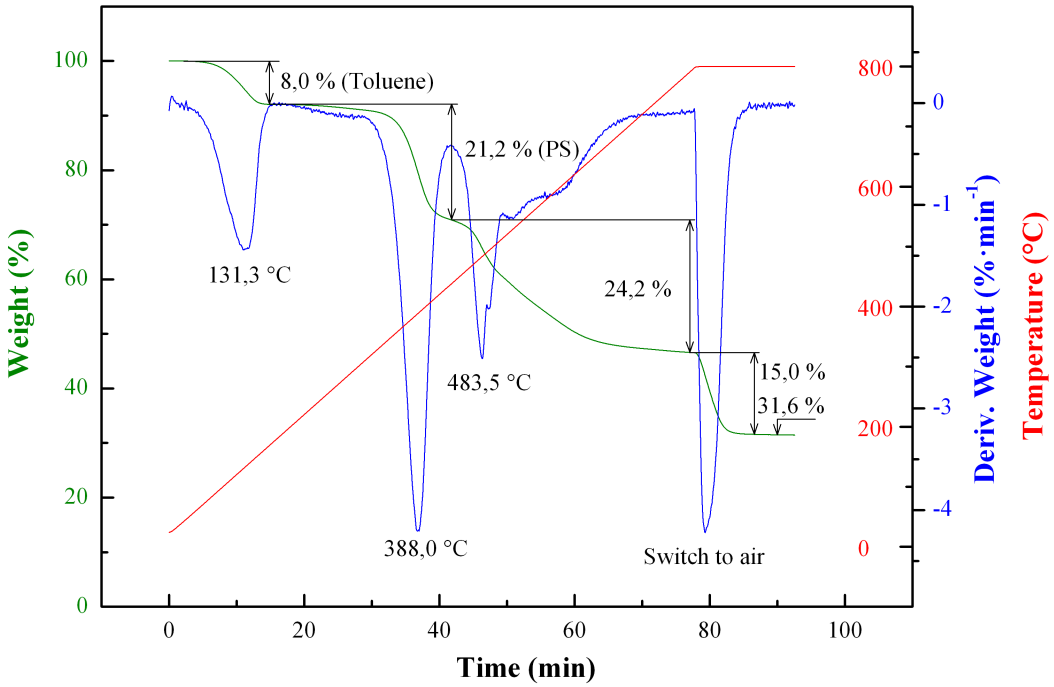

Fig. 17: Thermogravimetric analysis of OP-POSS/PS masterbatch

4.2.2. Fourier transform infrared spectroscopy

IR spectra of pure OP-POSS and OM-POSS were recorded and the peaks were assigned to specific moieties as presented in Fig. 18 and Fig. 19 respectively. In the case of OP-POSS, aromatic cycles provide the strongest signal and according to the tabulated ranges, silicon atom attached to aromatic cycle cause slight shift in wavelength range where the peaks occur. Since aromatic cycles are present also in PS, the small differences in wavelength led in most cases to one broadened peak in OP-POSS/PS nanocomposites even for higher OP-POSS loadings. Therefore the attention was focused only on several peaks which clearly do not belong to PS spectrum, namely peaks at 500, 608, 1092 and 1136 cm^{-1}.

Similarly to TGA, FTIR proved low sensibility to nanocomposites with POSS loadings below 1,0 wt.% with only trace evidence of the strongest peaks which cannot be unambiguously attributed to the POSS. The FTIR spectra of OP-POSS nanocomposites are visualized in Fig. 20 with a detailed view of the wavelength range 1300–500 cm^{-1} in Fig. 21. Despite both TGA and FTIR did not distinguish low loadings of POSS, a proof of its presence in the samples is provided in the chapter 4.2.5.

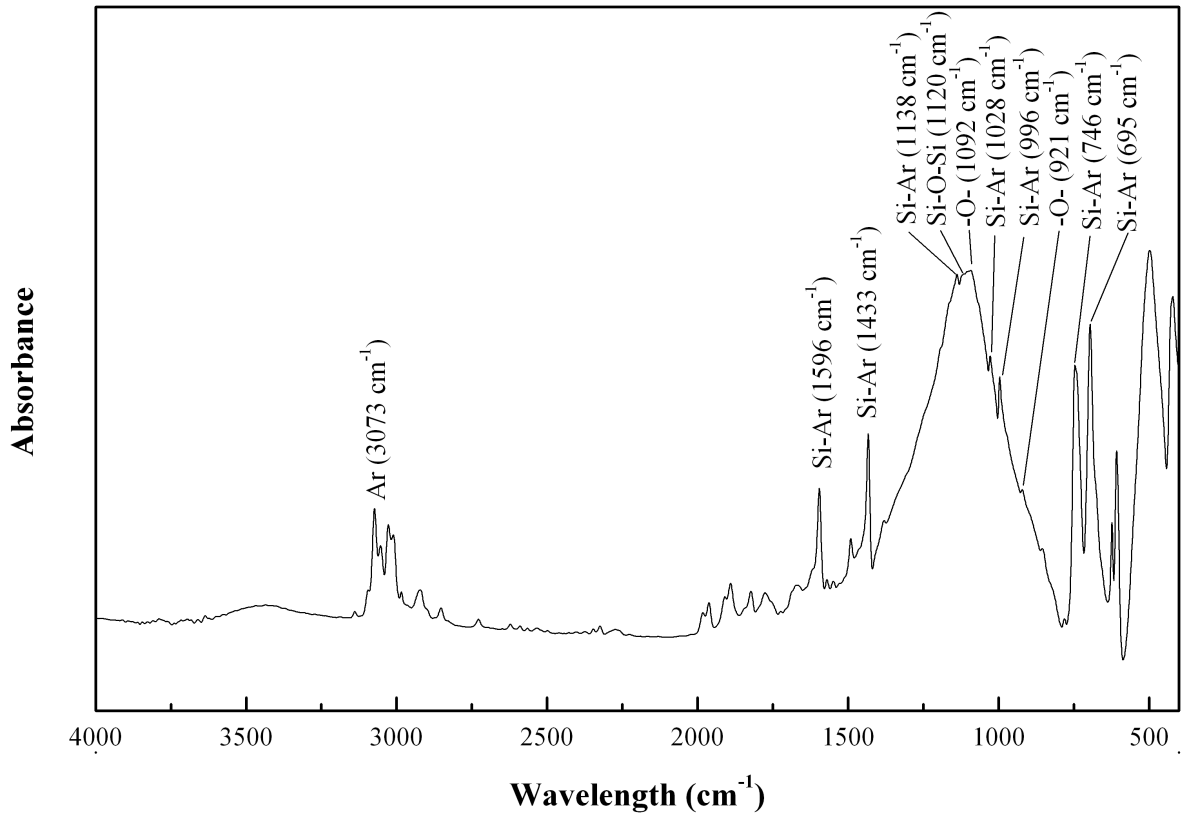

Fig. 18: FTIR spectrum of OP-POSS

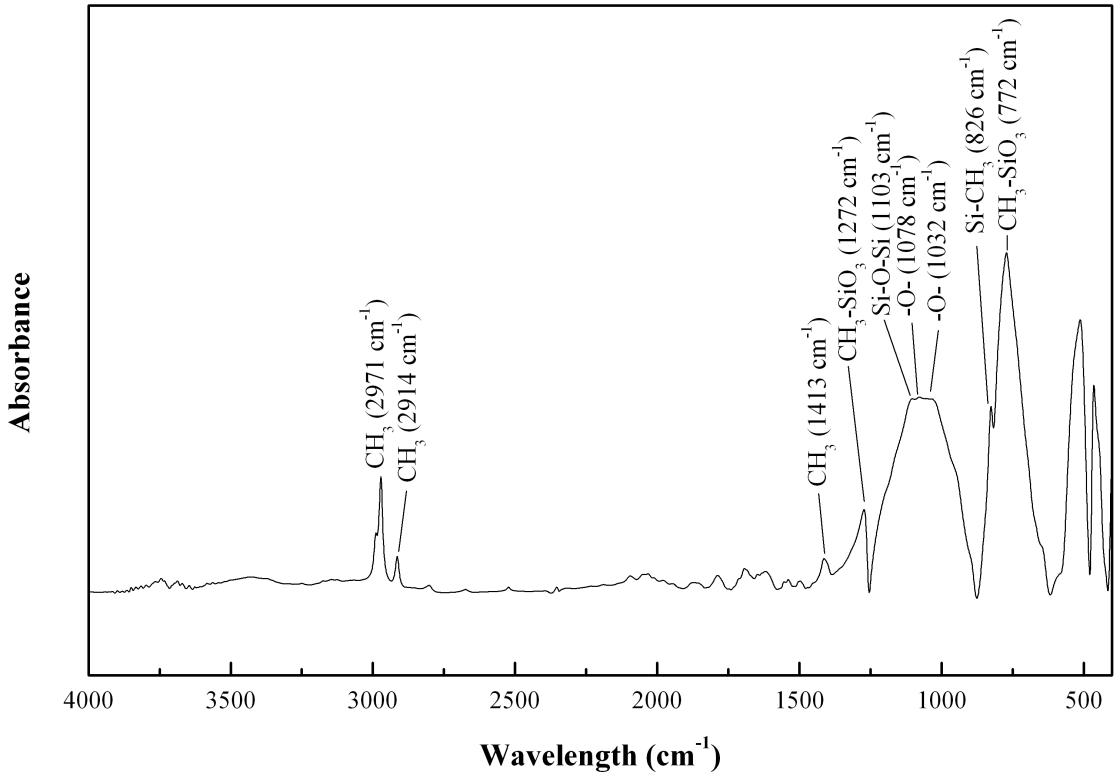

Fig. 19: FTIR spectrum of OM-POSS

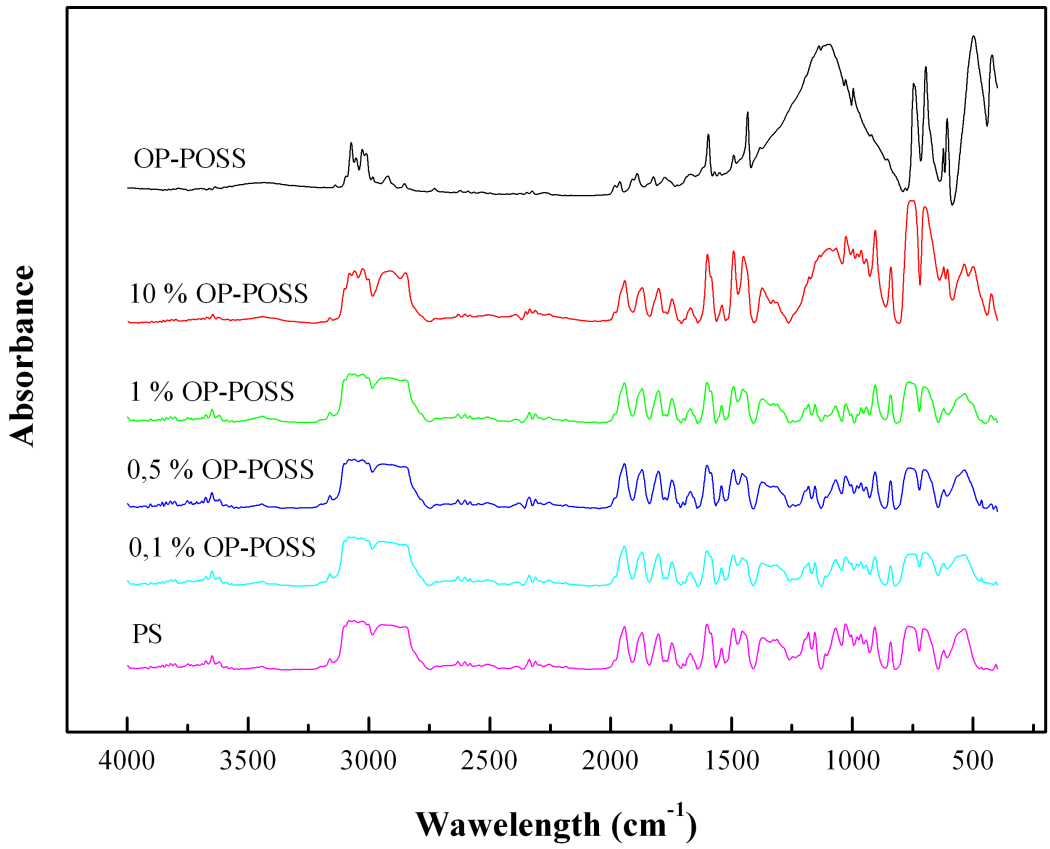

Fig. 20: FTIR spectra of OP-POSS/PS nanocomposites

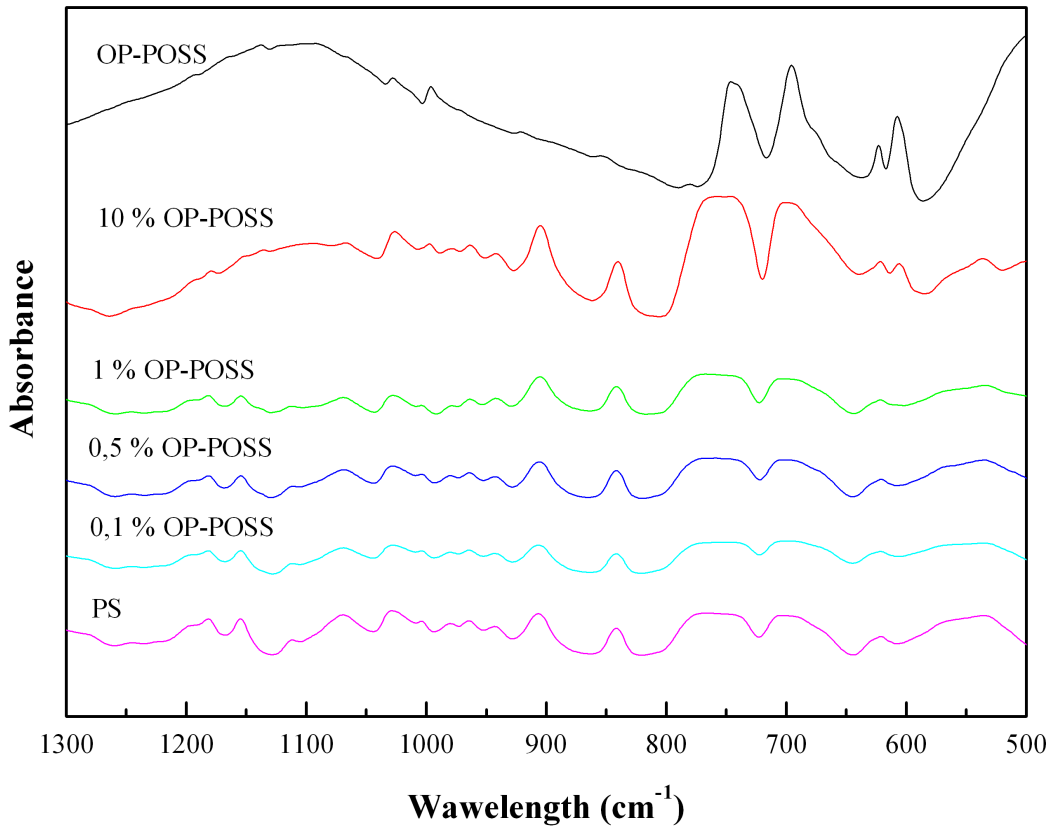

Fig. 21: FTIR spectra of OP-POSS/PS nanocomposites - detailed view of the range 1300–500 cm^{-1}

4.2.3. Microscopy

The applied procedure of nanocomposite sheet preparation led to microscale inhomogeneities when 10 wt.% OP-POSS was added into PS whereas samples with 1, 0,5 and 0,1 wt.% remained transparent. Fig. 22 shows CLSM pictures of these inhomogeneities which resemble scratches on the sheet surface which might be caused by the particles during the pressure molding. It suggests that OP-POSS is well miscible with PS at low filler ratios whereas 10 wt.% exceeds the miscibility threshold. Similar inhomogeneities were observed in OM-POSS/PS and OP-POSS/PMMA nanocomposites where low compatibility was also expected.

Indeed, structures with size of hundreds of nanometers were found in 10 % OP-POSS/PS nanocomposite by SEM (see Fig. 23); however, it is important to note that without chemical element mapping these structures cannot be unambiguously attributed to the OP-POSS particles. Presence or absence of silicon in these structures will confirm or disprove their connection with silsesquioxanes as well as it could prove partial miscibility of OP-POSS with PS on nano-scale if silicon will be found homogenously distributed throughout the matrix. Although it will be a subject of further research, the results were not available up-to-date and therefore were excluded from this thesis. It should be noted that the black shadow visible in Fig. 23A is caused by deposition of a surface pollution layer on the specimen under the electron beam exposure in the low vacuum and cannot be interpreted as a part of the sample's morphology.

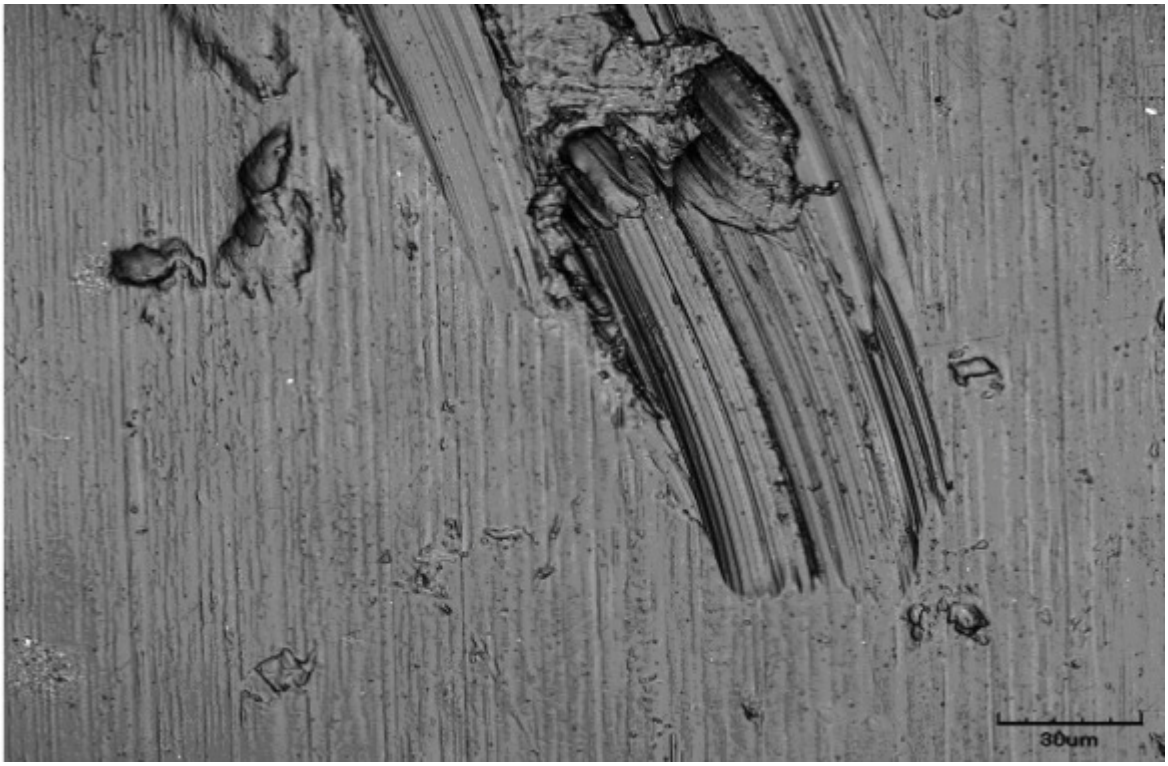

Fig. 22: Inhomogeneities in 10 % OP-POSS/PS nanocomposite sheet pictured with confocal laser scanning microscope

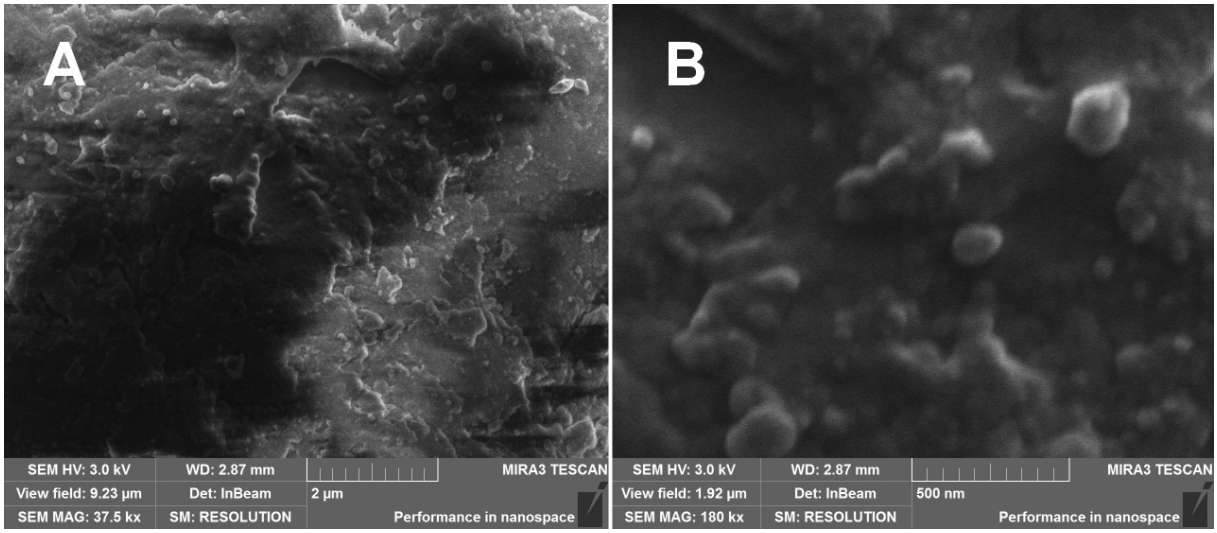

Fig. 23: SEM images of 10 % OP-POSS/PS nanocomposite A) at magnification 37 500× B) at magnification 180 000×

4.2.4. Thermomechanic behavior

Although a single-cantilever DMA setup is generally recommended for thermoplastic polymers, tensile DMA measurements were chosen to fit the optimal measuring range of the utilized device due to constraints to the specimen geometry preparation. The strain sweep test were conducted to establish the strain amplitude 0,02 % from the linear region for the temperature ramp measurements, the dependence of storage modulus on strain for 1,0 % OP-POSS is presented as an example in Fig. 24. The temperature dependence of storage and loss moduli of OP-POSS nanocomposites is displayed in Fig. 25.

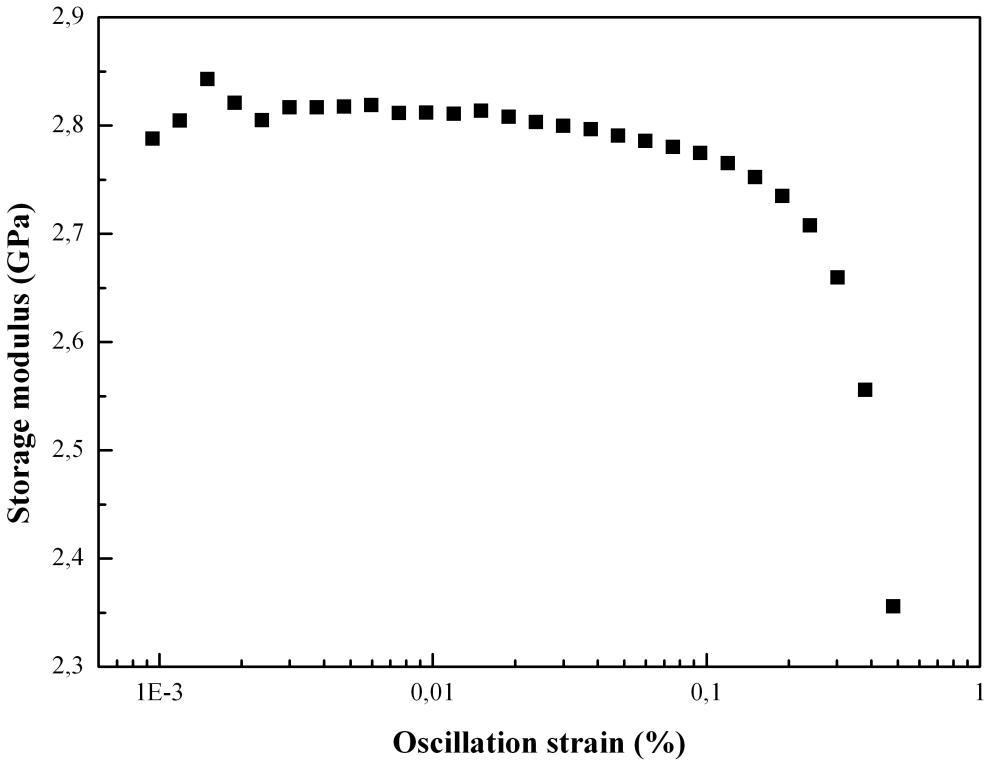

Fig. 24: DMA strain sweep measurement of 1,0 % OP-POSS/PS

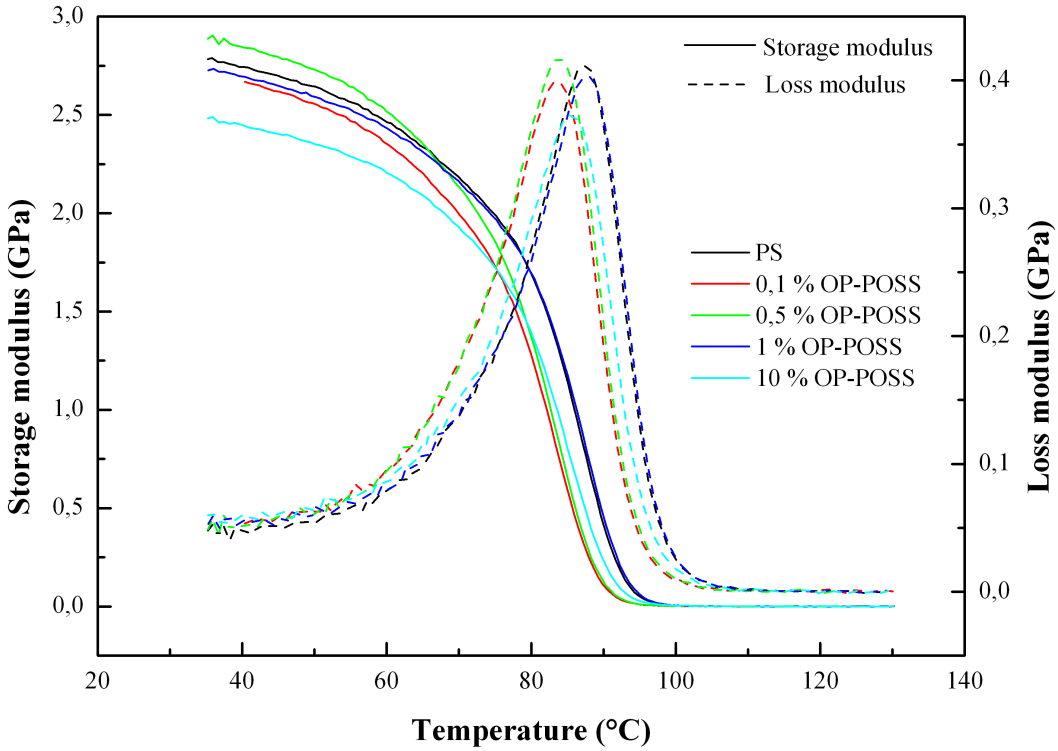

Fig. 25: Thermomechanic spectra of OP-POSS/PS nanocomposites

The glass transition temperature T_g was found from the maximum of loss modulus and the established value 87,7 °C for blank PS matches reasonably well with 87,5 °C measured by DSC. Addition of OP-POSS led to a slight decrease in T_g (up to 5,2 °C); however, the lowest value 83,6 °C (82,0 °C by DSC) was determined for the lowest loading of OP-POSS. It implies that low loadings 0,1 % and 0,5 % change thermomechanic behavior more than higher

loadings 1,0 % and 10 %. The decrease in T_g could be attributed to dispersed nanoparticles whereas particles above the critical size never soften the polymer. Intuitively, bigger agglomerates are generally expected at higher filler ratios; however, decrease in both the storage modulus below T_g and the maximum in the loss modulus could be found at 10 % of OP-POSS, which could be related to the presence of the microscale-defects found in these samples. At 1,0 wt.%, T_g did not significantly differ between OP-POSS and OM-POSS. DSC and DMA measurements did not correlate so well in case of PMMA, DMA distinguished no difference in T_g between 1,0 % OP-POSS/PMMA nanocomposite and blank sample whereas difference 5,9 °C was recorded by DSC. An overview of all gathered T_g is summed up in Table 1.

Table 2: Glass transition temperature of POSS nanocomposites (°C)

	DSC			**DMA**		
	PS		**PMMA**	**PS**		**PMMA**
	OP-POSS	**OM-POSS**	**OP-POSS**	**OP-POSS**	**OM-POSS**	**OP-POSS**
0 %	87,5		100,3	87,7		84,8
0,1 %	82,0			83,6		
0,5 %	82,8			84,4		
1,0 %	85,6	83,9	94,6	88,4	84,1	84,8
10 %	84,5			84,3		

4.2.5. Rheology

Comparison of OP-POSS/PS nanocomposites solutions at concentrations 1 g per 2,5 ml toluene and 1 g per 5,0 ml toluene is provided in Fig. 26. Increase in both storage and loss moduli was obtained for solution with higher concentration as expected; however, two non-linear steps were found in the applied strain range (for the lower concentration solution, see the detail in Fig. 27). The first one at strain of approximately 10 % exhibits yield point behavior with storage modulus drop and maximum in loss modulus. The second is shifted to lower strains one order of magnitude as the concentration increases and both storage and loss moduli drop to near zero values. The behavior could be explained by formation of different structures, if one assumes that bigger structures are more rigid thus they contribute more to the moduli and simultaneously, they exhibit higher formation time. Since the strain of the oscillatory test increases and the frequency is kept constant, strain rate increases and when threshold is reached, the bigger structures lack time to form and their contribution is suppressed. Addition of OP-POSS has no substantial effect on these changes; however, if one consider the assumption described above, they probably influence the formed structures and thus alter the moduli in particular regions.

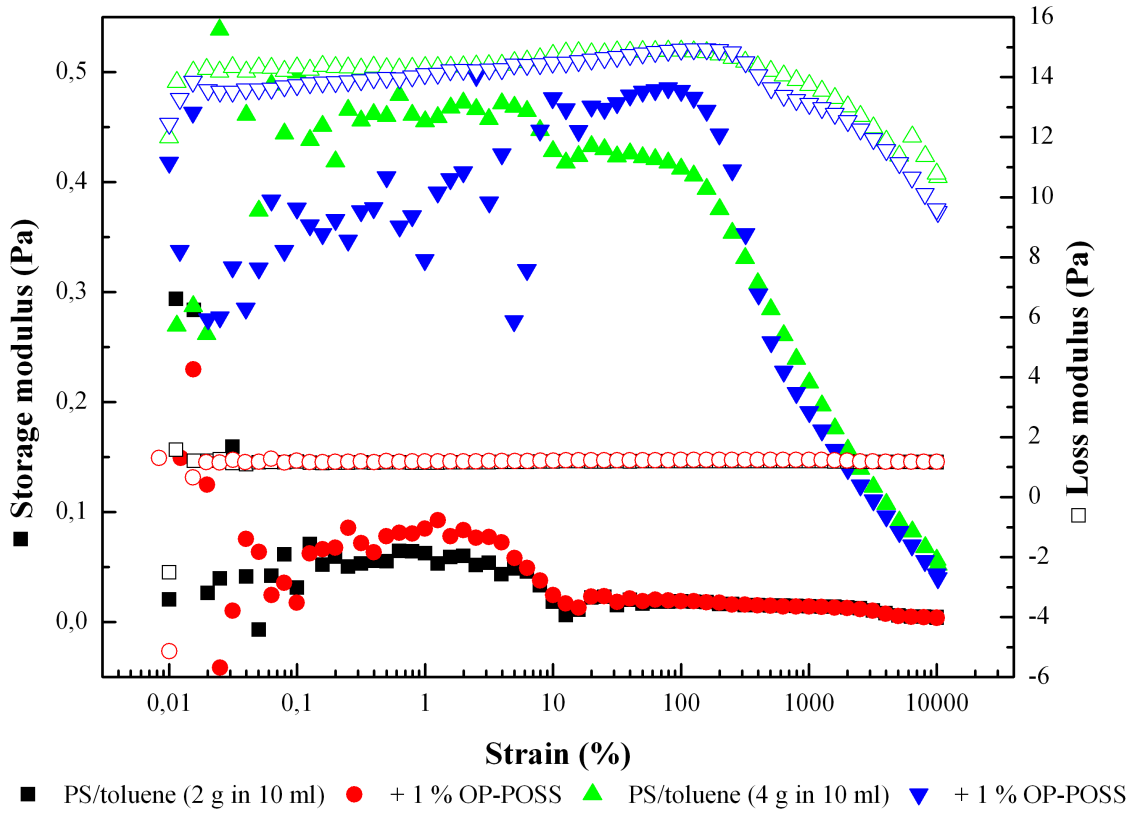

Fig. 26: OP-POSS/PS solution in toluene storage and loss moduli dependence on strain at various concentrations

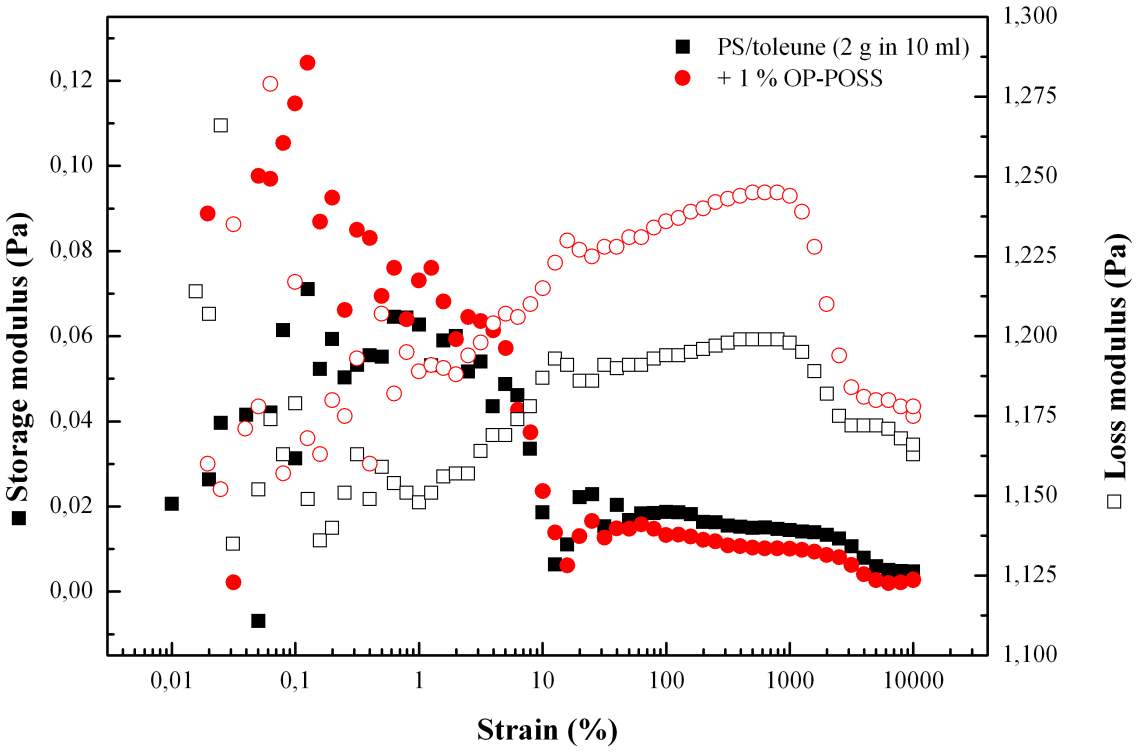

Fig. 27: Storage and loss modulus dependence on strain for OP-POSS/PS solution in toluene (2 g in 10 ml of solvent) compared to pure PS solution

Loss and storage moduli dependence on strain of OP-POSS/PS nanocomposites solution in toluene (1 g per 2,5 ml solvent) are summarized in Fig. 28 and Fig. 29 respectively. They clearly evidence that addition of OP-POSS into PS solution leads to increase in both loss and storage moduli of the system with increasing strain, especially in the middle range of strain. The effect weakened with increasing OP-POSS concentration which would mean atypical anti-Stokes-Einstein behavior if bigger OP-POSS agglomerates are supposed for higher loadings what could be described by role of dispersed particles on polymer chains dynamics. The amount of the dispersed OP-POSS might decrease when agglomeration is favored. Another possible explanation is a strain induced particle association but in this case, one would expect increasing tendency with increasing filler ratio.

OM-POSS/PS and OP-POSS/PMMA solutions in toluene were investigated to compare the nanofiller contribution in different systems. Fig. 30 compares the contribution of OP-POSS and OM-POSS at 1 wt.% in respect to PS. Both types of POSS result in increase in storage modulus but the OP-POSS contribution overweight the OM-POSS contribution and in the middle region it even exceeds values obtained for the blank system. Since higher affinity of PS to OP-POSS than to OM-POSS is expected, this results further suggest the effect of attractive nanoparticles to polymer chain dynamics as described above.

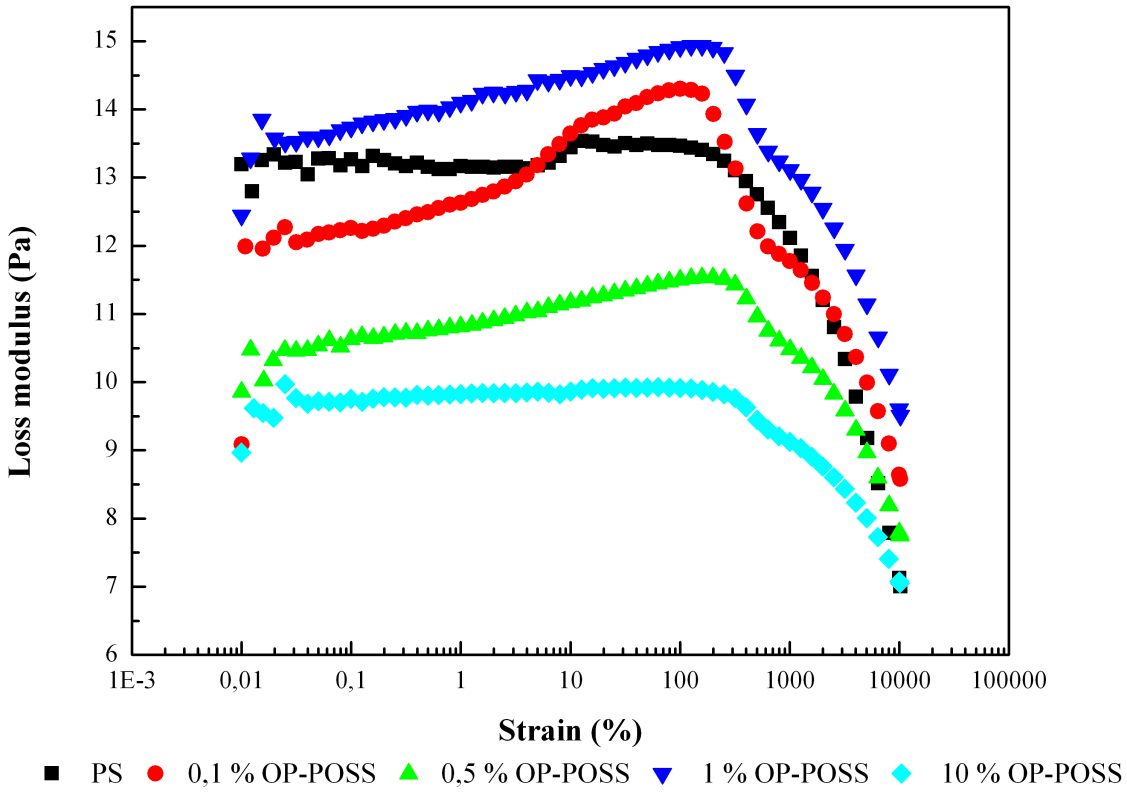

Fig. 28: Dependence of loss modulus on strain for OP-POSS/PS nanocomposites (1 g in 2,5 ml toluene)

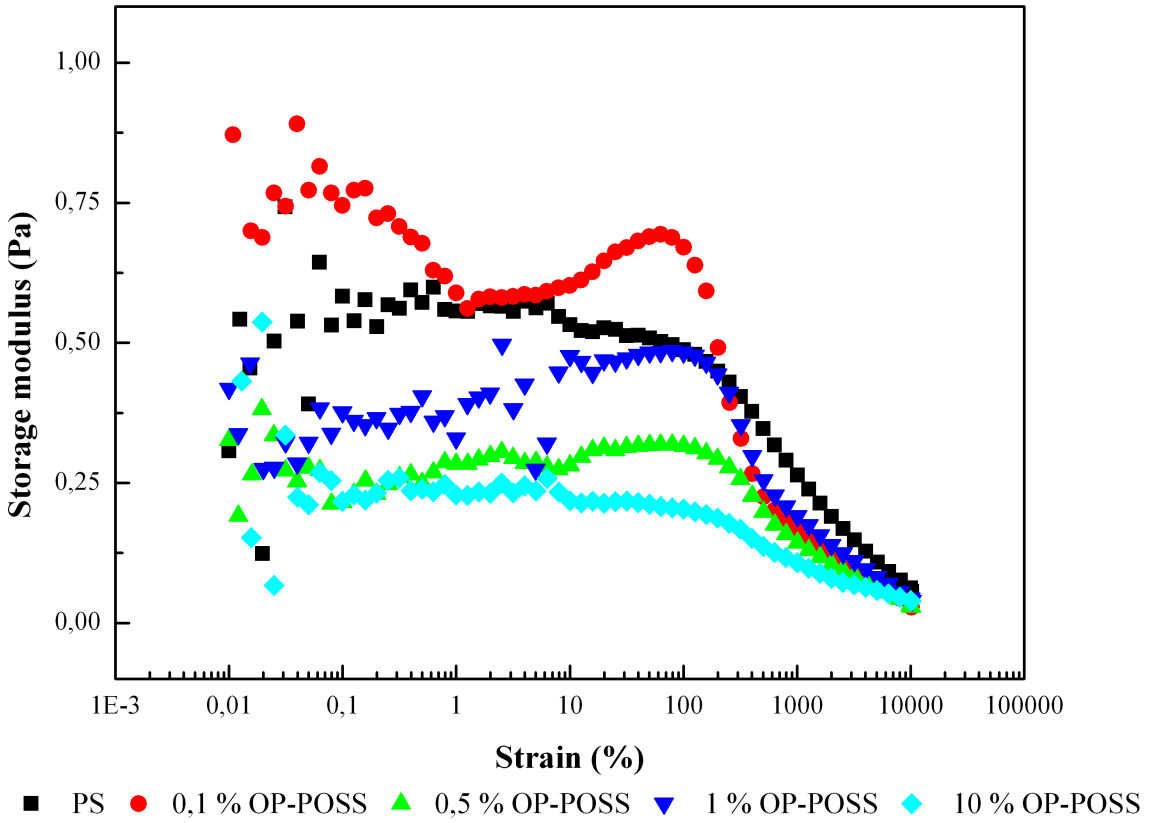

Fig. 29: Dependence of storage modulus on strain for OP-POSS/PS nanocomposites (1 g in 2,5 ml toluene)

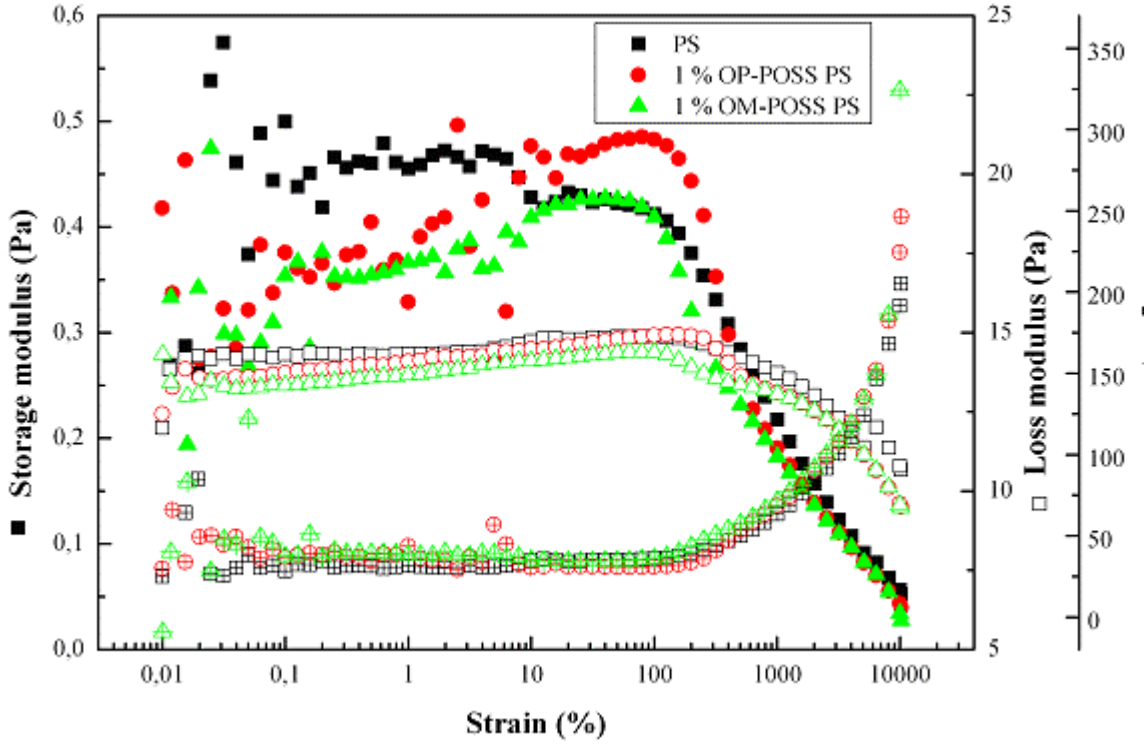

Fig. 30: Comparison of rheological behavior of OP-POSS/PS and OM-POSS/PS solution in toluene

PMMA solution in toluene exhibited behavior significantly different to PS with peak in both storage and loss moduli in the middle strain range as displayed in Fig. 31. In solution, such response might be attributed to an increase in the effective hydrodynamic volume which is known for instance for polymer association induced by shear. Moreover, the range where it occurs corresponds with the range of non-linear behavior in PS solution. The peak is preserved in the presence of 1 wt.% OP-POSS which caused increased values of both storage and loss moduli; however, the increase were suppressed in high-strain region.

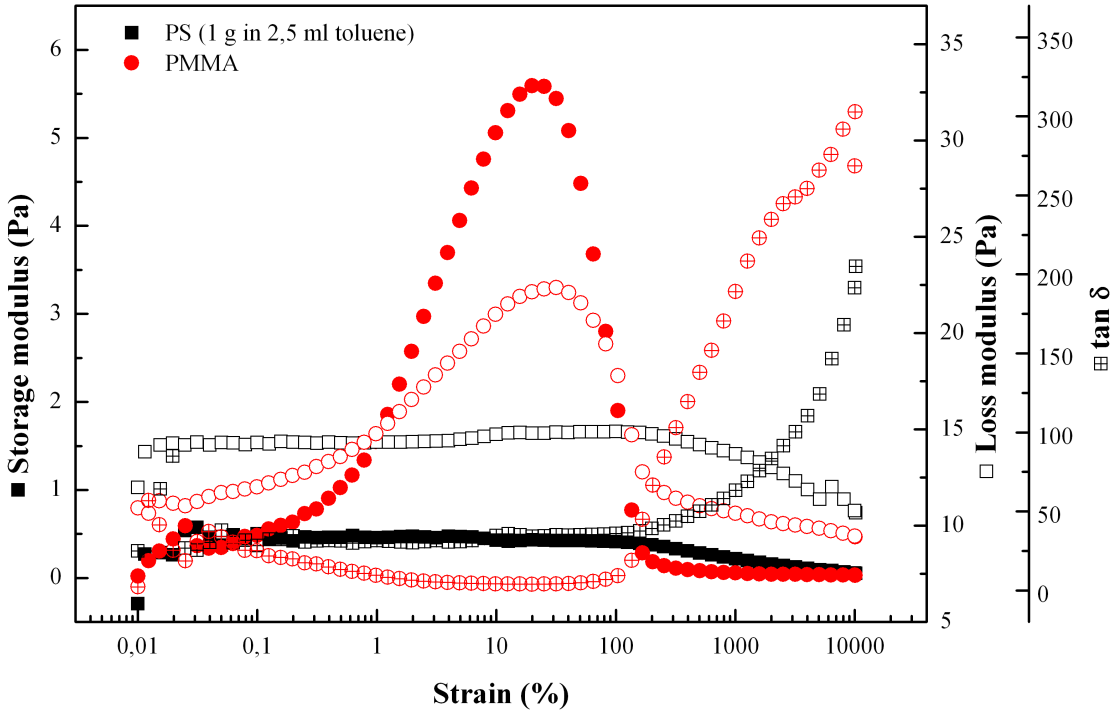

Fig. 31: Rheological behavior of PMMA and PS solutions in toluene

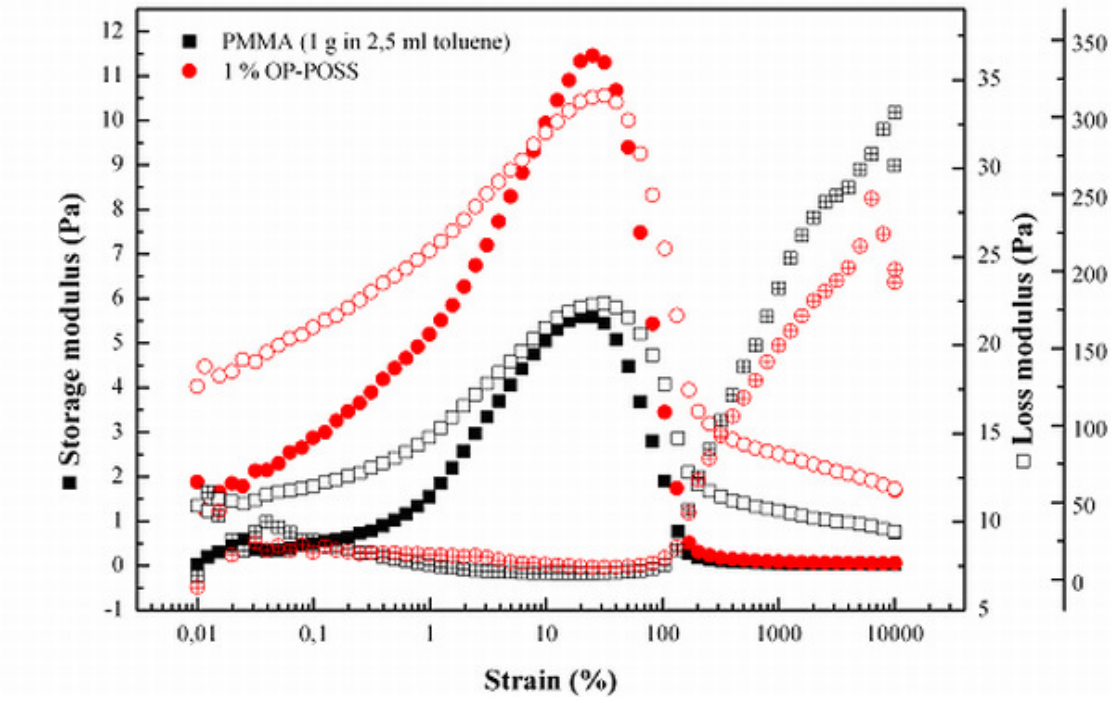

Fig. 32: Influence of OP-POSS addition on PMMA solution in toluene rheological response

5. CONCLUSION

The effects of preparation protocol for polyhedral oligomeric silsesquioxanes (POSS) based polymer nanocomposites through solution blending were found and described as one of the main goals of this thesis. Particularly, OP-POSS/PS, OM-POSS/PS and OP-POSS/PMMA systems were studied. Initial tests with POSS suspensions revealed that the OP-POSS nanoparticle size is weakly dependent on varying toluene-acetone ratio thus assuming low direct influence of the solvent on the particle spatial organization.

Due to the achieved transparency of the pressure molded sheets, it was concluded that the procedure yields good POSS particle dispersion for low loadings of OP-POSS in polystyrene, whereas, 10 wt.% of OP-POSS led to microscale inhomogeneities and reduced transparency. In the same sample, but, before subjecting to the pressure molding, structures with size of hundred nanometers where found with SEM. Chemical element mapping focused on silicon will be carried out to confirm or reject their relation to OP-POSS. Systems OP-POSS/PMMA and OM-POSS/PS, where lower filler-matrix affinity was expected also resulted in reduced transparency of the pressure molded sheets.

TGA was used to evaluate POSS content in masterbatches which were used for preparation of different concentration nanocomposites, but it proved to be not reliable for low POSS concentrations. FTIR was also not sufficiently reliable for low POSS concentrations. The presence of POSS in the nanocomposites was evidenced by increasing intensity of milky haze appearance of their solutions in toluene and rheology of these solutions was studied. Non-linear behavior with three regions was revealed in blank samples and the position of these regions was preserved after addition of POSS in all studied systems. POSS presence caused storage and loss moduli increase with increasing strain in first two regions whereas the high-strain region was only weakly altered by the presence of POSS. A possible explanation considers formation of various structures which contribute to storage and loss moduli. With increasing shear rate, the formation of larger structures is suppressed and its contribution to stiffness vanishes. Other results also support the hypothesis that dispersed attractive nanoparticles alter the matrix chain dynamics and lead to higher values of storage and loss moduli.

Thermomechanical measurements found reasonable agreement between glass transition temperature determined by DSC and DMA. Surprisingly, in the PS systems, the biggest difference of 5,2 °C was found for the lowest applied OP-POSS loading. That suggests that influence of the state of dispersion exceeds the filler volume contribution to T_g.

REFERENCES

1. JANCAR, J., J. F. DOUGLAS, F. W. STARR, S. K. KUMAR, P. CASSAGNAU, A. J. LESSER, S. S. STERNSTEIN and M. J. BUEHLER. Current issues in research on structure–property relationships in polymer nanocomposites. *Polymer*. 2010, vol. 51, issue 15, p. 3321-3343.
2. KOPESKY, E. T., T. S. HADDAD, G. H. MCKINLEY and R. E. COHEN. Miscibility and viscoelastic properties of acrylic polyhedral oligomeric silsesquioxane–poly(methyl methacrylate) blends. *Polymer*. 2005, vol. 46, issue 13, p. 4743-4752.
3. DORIGATO, A., Y. DZENIS and A. PEGORETTI. Filler aggregation as a reinforcement mechanism in polymer nanocomposites. *Mechanics of Materials*. 2013, vol. 61, p. 79-90.
4. SCHÄFER, B., M. HECHT, J. HARTING a H. NIRSCHL. Agglomeration and filtration of colloidal suspensions with DVLO interactions in simulation and experiment. *Journal of Colloid and Interface Science*. 2010, vol. 349, issue 1, s. 186-195.
5. YAN, L.-T. and X.-M. XIE. Computational modeling and simulation of nanoparticle self-assembly in polymeric systems: Structures, properties and external field effects. *Progress in Polymer Science*. 2013, vol. 38, issue 2, p. 369-405.
6. TORQUATO, S. and Y. JIAO. Organizing principles for dense packings of nonspherical hard particles: Not all shapes are created equal. *Physical Review E*. 2012, vol. 86, issue 1, p. 011102-1–011102-14.
7. STARR, F. W., J. F. DOUGLAS and S. C. GLOTZER. Origin of particle clustering in a simulated polymer nanocomposite and its impact on rheology. *The Journal of Chemical Physics*. 2003, vol. 119, issue 3, p. 1777-1788.
8. MOLINA-BOLÍVAR, J. A., F. GALISTEO-GONZÁLEZ and R. HIDALGO-ALVAREZ. The role played by hydration forces in the stability of protein-coated particles: non-classical DLVO behaviour. *Colloids and Surfaces B: Biointerfaces*. 1999, vol. 14, 1-4, p. 3-17.
9. SHENHAR, R., T. B. NORSTEN and V. M. ROTELLO. Polymer-Mediated Nanoparticle Assembly: Structural Control and Applications. *Advanced Materials*. 2005-03-22, vol. 17, issue 6, p. 657-669.
10. HOOPER, J. B. a K. S. SCHWEIZER. Theory of Phase Separation in Polymer Nanocomposites. *Macromolecules*. 2006, vol. 39, issue 15, s. 5133-5142.
11. ANDERSON, B. J. and C. F. ZUKOSKI. Rheology and Microstructure of Polymer Nanocomposite Melts: Variation of Polymer Segment−Surface Interaction. *Langmuir*. 2010, vol. 26, issue 11, p. 8709-8720.
12. PATRA, T. K. and J. K. SINGH. Coarse-grain molecular dynamics simulations of nanoparticle-polymer melt: Dispersion vs. agglomeration. *The Journal of Chemical Physics*. 2013, vol. 138, issue 14, p. 144901-7.
13. RAHEDI, A. J., J. F. DOUGLAS and F. W. STARR. Model for reversible nanoparticle assembly in a polymer matrix. *The Journal of Chemical Physics*. 2008, vol. 128, issue 2, p. 024902-9.
14. TANTISHAIYAKUL, V., N. WORAKUL a W. WONGPOOWARAK. Prediction of solubility parameters using partial least square regression. *International Journal of Pharmaceutics*. 2006, vol. 325, 1-2, s. 8-14.

15. KIM, S. Y. and C. F. ZUKOSKI. Role of Polymer Segment–Particle Surface Interactions in Controlling Nanoparticle Dispersions in Concentrated Polymer Solutions. *Langmuir*. 2011-09-06, vol. 27, issue 17, p. 10455-10463.
16. KALRA, V., F. ESCOBEDO and Y. L. JOO. Effect of shear on nanoparticle dispersion in polymer melts: A coarse-grained molecular dynamics study. *The Journal of Chemical Physics*. 2010, vol. 132, issue 2, p. 024901-11.
17. LIU, J., Y. GAO, D. CAO, L. ZHANG and Z. GUO. Nanoparticle Dispersion and Aggregation in Polymer Nanocomposites: Insights from Molecular Dynamics Simulation. *Langmuir*. 2011-06-21, vol. 27, issue 12, p. 7926-7933.
18. BONCHEVA, M. and G. M. WHITESIDES. 4. Biomimetic Approaches to the Design of Functional, Self-Assembling Systems. *Dejjer Encyclopedia of Nanoscience and Nanotechnology*. 2004, p. 287-294.
19. AGGELI, A., I. A. NYRKOVA, M. BELL, R. HARDING, L. CARRICK, T. C. B. MCLEISH, A. N. SEMENOV and N. BODEN. Hierarchical self-assembly of chiral rod-like molecules as a model for peptide -sheet tapes, ribbons, fibrils, and fibers. *Proceedings of the National Academy of Sciences*. 2001-10-09, vol. 98, issue 21, p. 11857-11862.
20. AKCORA, P., H. LIU, S. K. KUMAR, J. MOLL, Y. LI, B. C. BENICEWICZ, L. S. SCHADLER, D. ACEHAN, A. Z. PANAGIOTOPOULOS, V. PRYAMITSYN, V. GANESAN, J. ILAVSKY, P. THIYAGARAJAN, R. H. COLBY and J. F. DOUGLAS. Anisotropic self-assembly of spherical polymer-grafted nanoparticles. *Nature Materials*. 2009-3-22, vol. 8, issue 4, p. 354-359.
21. KUMAR, S. K., N. JOUAULT, B. BENICEWICZ and T. NEELY. Nanocomposites with Polymer Grafted Nanoparticles. *Macromolecules*. 2013-05-14, vol. 46, issue 9, p. 3199-3214.
22. BANEY, M. ITOH, A. SAKAKIBARA and T. SUZUKI. Silsesquioxanes. *Chem. Rev.* 1995, vol. 95, issue 5, p. 1409–1430.
23. KUO, S.-W. and F.-C. CHANG. POSS related polymer nanocomposites. *Progress in Polymer Science*. 2011, vol. 36, issue 12, p. 1649-1696.
24. HYBRID PLASTICS. *POSS User's Guide*. version 2.06. 2013. Available at: http://www.hybridplastics.com/docs/user-v2.06.pdf
25. FRYE, C. L. and W. T. COLLINS. Oligomeric silsesquioxanes, $(HSiO_{3/2})_n$. *Journal of the American Chemical Society*. 1970, vol. 92, issue 19, p. 5586-5588.
26. AGASKAR, P. A. New synthetic route to the hydridospherosiloxanes O_h-$H_8Si_8O_{12}$ and D_{5h}-$H_{10}Si_{10}O_{15}$. *Inorganic Chemistry*. 1991, vol. 30, issue 13, p. 2707-2708.
27. BARRY, A. J., W. H. DAUDT, J. J. DOMICONE and J. W. GILKEY. Crystalline Organosilsesquioxanes. *Journal of the American Chemical Society*. 1955, vol. 77, issue 16, p. 4248-4252.
28. MARCOLLI, C. a G. CALZAFERRI. Monosubstituted Octasilasesquioxanes. *Applied Organometallic Chemistry*. 1999, vol. 13, issue. 4, p. 213-226.
29. TSUCHIDA, A., C. BOLLN, F. G. SERNETZ, H. FREY and R. MÜLHAUPT. Ethene and Propene Copolymers Containing Silsesquioxane Side Groups. *Macromolecules*. 1997, vol. 30, issue 10, p. 2818-2824.

30. DAY, V. W., Walter G. KLEMPERER, V. V. MAINZ and D. M. MILLAR. Molecular building blocks for the synthesis of ceramic materials: $[Si_8O_{12}](OCH_3)_8$. *Journal of the American Chemical Society*. 1985, vol. 107, issue 26, p. 8262-8264.
31. BROWN, J. F. a Lester H. VOGT. The Polycondensation of Cyclohexylsilanetriol. *Journal of the American Chemical Society*. 1965, vol. 87, issue 19, p. 4313-4317.
32. FEHER, F. J., T. A. BUDZICHOWSKI, K. RAHIMIAN and J. W. ZILLER. Reactions of incompletely-condensed silsesquioxanes with pentamethylantimony: a new synthesis of metallasilsesquioxanes with important implications for the chemistry of silica surfaces. *Journal of the American Chemical Society*. 1992, vol. 114, issue 10, p. 3859-3866.
33. LICHTENHAN, J. D., N. Q. VU, J. A. CARTER, J. W. GILMAN and F. J. FEHER. Silsesquioxane-siloxane copolymers from polyhedral silsesquioxanes: a new synthesis of metallasilsesquioxanes with important implications for the chemistry of silica surfaces. *Macromolecules*. 1993, vol. 26, issue 8, p. 2141-2142.
34. PHILLIPS, S. H., T. S. HADDAD and S. J. TOMCZAK Developments in nanoscience: polyhedral oligomeric silsesquioxane (POSS)-polymers. *Current Opinion in Solid State and Materials Science*. 2004, vol. 8, issue 1, p. 21-29.
35. MISRA, R., A. H. ALIDEDEOGLU, W. L. JARRETT and S. E. MORGAN. Molecular miscibility and chain dynamics in POSS/polystyrene blends: Control of POSS preferential dispersion states. *Polymer*. 2009, vol. 50, issue 13, p. 2906-2918.
36. SÁNCHEZ-SOTO, M., D. A. SCHIRALDI and S. ILLESCAS. Study of the morphology and properties of melt-mixed polycarbonate–POSS nanocomposites. *European Polymer Journal*. 2009, vol. 45, issue 2, p. 341-352.
37. FINA, A., D. TABUANI, A. FRACHE and G. CAMINO. Polypropylene–polyhedral oligomeric silsesquioxanes (POSS) nanocomposites. *Polymer*. 2005, vol. 46, issue 19, p. 7855-7866.
38. JEON, H. G., P. T. MATHER and T. S. HADDAD. Shape memory and nanostructure in poly(norbornyl-POSS) copolymers. *Polymer International*. 2000, vol. 49, issue. 5, p. 453-457.
39. PERRIN, F. X., D. M. PANAITESCU, A. N. FRONE, C. RADOVICI and C. NICOLAE. The influence of alkyl substituents of POSS in polyethylene nanocomposites. *Polymer*. 2013, vol. 54, issue 9, p. 2347-2354.
40. COLEMAN, M. and P. PAINTER. Hydrogen bonded polymer blends. *Progress in Polymer Science*. 1995, vol. 20, issue 1, p. 1-59.
41. IYER, S. and D. A. SCHIRALDI. Role of Specific Interactions and Solubility in the Reinforcement of Bisphenol A Polymers with Polyhedral Oligomeric Silsesquioxanes. *Macromolecules*. 2007, vol. 40, issue 14, p. 4942-4952.
42. RAHMAN, M., V. FILIZ, S. SHISHATSKIY, C. ABETZ, S. NEUMANN, S. BOLMER, M. M. KHAN a Volker ABETZ. PEBAX® with PEG functionalized POSS as nanocomposite membranes for CO2 separation. *Journal of Membrane Science*. 2013, vol. 437, s. 286-297.
43. JOSHI, M., B. S. BUTOLA, G. SIMON a N. KUKALEVA. Rheological and Viscoelastic Behavior of HDPE/Octamethyl-POSS Nanocomposites. *Macromolecules*. 2006, vol. 39, issue 5, s. 1839-1849.
44. GOODWIN, James W. *Colloids and interfaces with surfactants and polymers: an introduction*. Hoboken, NJ: J. Wiley, c2004, vii, 285 p. ISBN 04-708-4143-5.

45. EHRENSTEIN, G. W. *Thermal analysis of plastics: theory and practice*. Munich: Hanser, 2004, 368 s. ISBN 34-462-2673-7.
46. CROMPTON, T. *Charalterisation of Polymers*. Shawbury: Smithers Rapra, 2008, x, 478 s. ISBN 978-1-84735-122-7.
47. TOLSTOY, Valeri P. *Handbook of infrared spectroscopy of ultrathin films*. Hoboken: Wiley-Interscience, 2003. ISBN 04-713-5404-X.
48. FLEWITT, P. and R WILD. *Physical methods for materials characterisation*. Philadelphia: Institute of Physics Pub., c1994, xvi, 517 p. ISBN 07-503-0320-4.
49. HANKE, L. D. MATERIALS EVALUATION AND ENGINEERING, Inc. *Handbook of Analytical methods for Materials*. Plymouth, 2001, 50 p.
50. MARCUS, Y. *The properties of solvents*. New York, c1998, xiv, 239 p. ISBN 04-719-8369-1.
51. SOCRATES, G. Infrared and raman characteristic group frequencies: tables and charts. 3rd ed. West Sussex: John Wiley, 2007. ISBN 04-700-9307-2.
52. ROEGES, N. P. A guide to the complete interpretation of infrared spectra of organic structures: tables and charts. 3rd ed. New York: Wiley, c1994, x, 340 p. ISBN 04-719-3998-6.
53. Spectool for Windows 2.1. *A Hypermedia Book for Structure Elucidation of Organic Compounds with Spectroscopic Methods*. Weinheim: Chemical Concepts, 1994.
54. LAUNER, P. J. Infrared analysis of organosilicon compounds: Spectra-structure correlations. In: ARKLES, B. *Silicon compounds: Register and review*. Bristol: Petrarch Systems, 1987, p. 100-103.

LIST OF SYMBOLS AND ABBREVIATIONS

α	constrained matrix volume ratio
δ	Dirac delta function
δ	Hansen's total solubility parameter
δ	shift angle (in DMA)
δ_d	dispersion contribution to Hansen's total solubility parameter
δ_h	hydrogen bond contribution to Hansen's total solubility parameter
δ_p	polar contribution to Hansen's total solubility parameter
tan δ	loss factor
ζ	zeta potential
η_0	viscosity
λ	wavelength
$\tilde{\nu}$	wavenumber
ρ	density
τ_c	correlation delay time
ϕ_A , ϕ_B	volume fractions of phases A and B
ϕ_f	filler volume fraction
ϕ_i	inclusion volume fraction
ϕ_m	matrix volume fraction
ϕ_{m1} , ϕ_{m2}	bulk and constrained matrix volume fractions
χ_{AB}	Flory–Huggins interaction parameter
ω	angular frequency
c	light velocity in vacuum
a_H	hydrodynamic radius of particle
C_A, C_B	concentrations (in mol·l^{-1})
CLSM	confocal laser scanning microscopy
d	interparticle center-to-center distance
D	particle diameter
D_s	self-diffusion coefficient of particle
DSC	differential scanning calorimetry
DMA	dynamic mechanical analysis
DVLO	Derjaguin–Landau–Verwey–Overbeek theory
E	elastic modulus
E^*	complex modulus
E'	storage modulus
E''	loss modulus
$\Delta E_{vap.}$	molar energy of vaporization
EDS	energy-dispersive x-ray spectroscopy
f	frequency
f_m^{OH}	fraction of free bond-donating group
FCC	face-centered cubic packing
FTIR	Fourier transform infrared spectroscopy
g	correlation function
G	shear modulus
$G(d)$	pair correlation function

ΔG_H	free energy of hydrogen bond formation
ΔG_m	free energy of mixing
HCP	hexagonal close packing
k_B	Boltzmann constant
K	effective bulk modulus
K_a	equilibrium constant for hydrogen bond association
IR	infrared
LD50	lethal dose, 50 %
LLDPE	linear low density polyethylene
M_A, M_B	degrees of polymerization
N	number of particles
PEG	polyethylene glycol
PMMA	poly(methyl methacrylate)
POSS	polyhedral oligomeric silsesquioxane
PS	polystyrene
R	universal gas constant
R_g	radius of gyration
Q	magnitude of scattering vector
SEM	scanning electron microscopy
T	thermodynamic temperature
T_7	incompletely condensed silsesquioxane structure with 7 silicon atoms
T_8	fully condensed silsesquioxane core with 8 silicon atoms
T_g	glass transition temperature
V	volume
V_m	molar volume
WDS	wavelength-dispersive x-ray spectroscopy
$\mathbf{x}_m$, $\mathbf{x}_n$	position vectors of particles m and n